J. Fluid Mech. (1992), *vol.* 245, *pp.* 523–551

Fully coupled resonant-triad interaction in an adverse-pressure-gradient boundary layer

By M. E. GOLDSTEIN[1] AND SANG SOO LEE[2]

[1] Lewis Research Center, Cleveland, OH 44135, USA

[2] Sverdrup Technology, Inc., Lewis Research Center Group, Cleveland, OH 44135, USA

(Received 30 August 1989 and in revised form 5 June 1992)

The nonlinear resonant-triad interaction, proposed by Raetz (1959), Craik (1971), and others for a Blasius boundary layer, is analysed here for an adverse-pressure-gradient boundary layer. We assume that the adverse pressure gradient is in some sense weak and, therefore, that the instability growth rate is small. This ensures that there is a well-defined critical layer located somewhere within the flow and that the nonlinear interaction is effectively confined to that layer. The initial interaction is of the parametric resonance type, even when the modal amplitudes are all of the same order. This means that the oblique instability waves exhibit faster than exponential growth and that the growth rate of the two-dimensional mode remains linear. However, the interaction and the resulting growth rates become fully coupled, once oblique-mode amplitudes become sufficiently large, but the coupling terms are now quartic, rather than quadratic as in the Craik (1971) analysis. More importantly, however, new nonlinear interactions, which were not present in the Craik-type analyses, now come into play. These interactions eventually have a dominant effect on the instability wave development.

1. Introduction

Subsonic boundary-layer transition experiments often involve spatially growing instability waves generated by nearly two-dimensional, single-frequency excitation devices such as vibrating ribbons or acoustic speakers. Experimentalists often go to great lengths to make the background disturbance level as small as possible in order to minimize the required external forcing levels. The resulting initial disturbances are then relatively two-dimensional, have harmonic time dependence and are well described by linear instability theory. This two-dimensional linear behaviour usually persists over very long streamwise distances in many of the more recent experiments where excitation levels tend to be quite small. However, the flow eventually becomes three-dimensional, as evidenced by the subsequent appearance of Λ-shaped structures in experiments where smoke-flow visualization is used. These structures, which are arranged in rows, can be aligned or can be staggered in alternating rows. The unstaggered arrangement, which was originally observed by Klebanoff, Tidstrom & Sargent (1962), is usually referred to as 'peak–valley' splitting.

The staggered arrangement, which tends to predominate at the lower excitation levels, is usually associated with a weak nonlinearity (Craik 1971; Smith & Stewart 1987) resulting from a resonant-triad interaction between a pair of oblique subharmonic modes (which frequently originate from the background disturbance environment) with the basic fundamental two-dimensional mode. This type of interaction was originally analysed for the case of viscous-dominated Tollmien–

Schlichting-type instabilities by Raetz (1959) and later by Craik (1971), who proposed that the unstaggered (or Klebanoff) arrangement (see Klebanoff *et al.* 1962) could also result from a resonant-triad interaction, which would then involve a pair of oblique fundamental harmonic modes interacting with the small two-dimensional instability mode that is invariably generated at the first harmonic of the excitation frequency (see §5.2 of Kachanov & Levchenko 1984 for a discussion of this issue).

Smith & Stewart (1987) attempted to put Craik's (1971) analysis on (what they consider to be) a more 'rational' basis by using triple-deck-type arguments, which they justify by noting that the Tollmien–Schlichting waves have a triple-deck structure in the vicinity of the lower branch of the neutral stability curve. This means that their results are focused on the case where nonlinearity comes into play at Reynolds number and frequency parameters beyond but still relatively close to the lower-branch neutral stability curve, where the critical layer is still within the viscous wall layer. Their result implies that this produces complete two-way coupling of the oblique and two-dimensional modes when the oblique-mode amplitude is of the same order as that of the plane wave.

These previous analyses were all concerned with viscous- or Tollmien–Schlichting-type instabilities. But transition in technological devices most often occurs in regions of adverse pressure gradient, and the onset of three-dimensionality typically occurs about four or five wavelengths upstream of the resulting transition point. The present paper therefore considers the case where the adverse pressure gradients are strong enough to produce essentially inviscid instabilities of the Rayleigh type. However, it is still appropriate to examine the limit of small adverse pressure gradient because even relatively small adverse pressure gradients (say, $O(R^{-\frac{1}{8}})$, where R denotes the Reynolds number based on downstream distance) can separate a laminar boundary layer (see e.g. Cheng & Smith 1982), in which case analyses of the present type would be largely irrelevant.

Of course, laminar boundary layers can also sustain order-one adverse pressure gradients, but even these tend to be numerically small. For example, separation occurs in the Falkner–Skan profiles when the Falkner–Skan exponent m, which directly corresponds to the negative of our normalized pressure gradient parameter μ defined in §2 below, is equal to -0.091 (Schlichting 1979, p. 165). Moreover, it is easy to show from the numbers given by Stewartson, Smith & Kaups (1982) that marginal separation is initiated on the 'leading-edge ellipse' of a thin airfoil when our pressure gradient parameter $\mu \approx 0.17$, which is remarkably close to the Falkner–Skan value.

We realize, of course, that there is a distinct difference between numerically and asymptotically small quantities and that the former definitely does not imply the latter in all cases. However, the numerically small adverse pressure gradient does suggest that the small-pressure-gradient asymptotic expansion will be a good approximation to the exact result right up to separation. Figure 1, which is a comparison of the numerical and asymptotic linear growth rates for a plane spatially growing instability wave on a Falkner–Skan profile, shows that this is indeed the case.

The linear growth rates are then small ($\propto$ (pressure gradient squared); see Goldstein, Durbin & Leib 1987), and the instability waves have a well-defined critical layer, but it is of the non-equilibrium (or growth-dominated) type rather than of the equilibrium (or viscous-dominated) type associated with Tollmien–Schlichting waves. This brings in a new non-equilibrium effect that does not occur in the analyses of Raetz (1959), Craik (1971), and Smith & Stewart (1987) and leads to a different

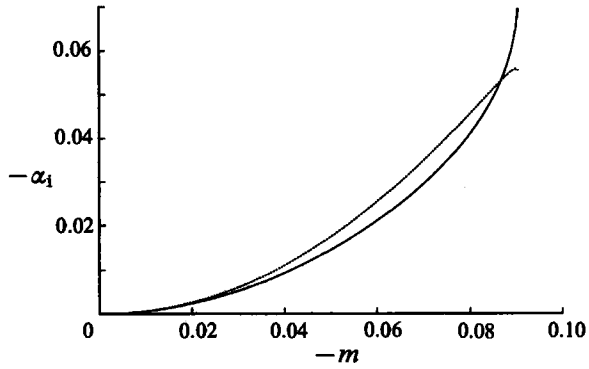

FIGURE 1. Maximum linear spatial growth rate of a plane mode, $-\alpha_1 \equiv A_x/A$, where

$$\tilde{x} = x((m+1)U/2\nu x)^{\frac{1}{2}},$$

as a function of the Falkner–Skan parameter; $U = cx^m$ (——, numerical; · · · · · ·, asymptotic). Both are computed at the same frequency which gives a maximum $-\alpha_1$ for the numerical solution.

type of amplitude equation that involves upstream history effects and is therefore an integro-differential equation (of the general type obtained by Hickernell 1984 in a somewhat different context, and by Goldstein & Choi 1989 in a more closely related context) rather than an ordinary differential equation (or, more accurately, a set of ordinary differential equations) as in the previous resonant-triad analyses. However, there are also much more important differences that arise because of a new type of nonlinear interaction that occurs in the present analysis but is absent in the previous studies of the resonant-triad interaction.

As in Smith & Stewart (1987), we attempt to develop a completely rational first-principles analysis. And, as in previous studies (e.g. Goldstein & Choi 1989), our interest is in the case where the nonlinear interactions arise from the continued downstream growth of a triad of initially linear instability waves: a single two-dimensional mode and two oblique modes with half the frequency and streamwise wavenumber of the two-dimensional mode and appropriate equal and opposite spanwise wavenumbers. These modes can then interact nonlinearly, with the nonlinearity first coming into play in the common critical layer of the three modes. The nonlinearity has a first-order effect on the (common) oblique-mode growth rate when the amplitude of the two-dimensional mode becomes of the order of that growth rate raised to the power $\frac{7}{2}$. But this initial nonlinearity is weak in the sense that it enters through an inhomogeneous term in a higher-order problem rather than as a coefficient in the lowest-order equation. The instability wave amplitude can then be determined explicitly from a set of amplitude equations (as in the Craik 1971 analysis) rather than implicitly through the numerical solution of a partial differential equation (as in the Gajjar & Smith 1985 and the Goldstein *et al.* 1987 analyses, for example). The amplitude equations are obtained by equating the critical-layer velocity jump as calculated from outside to the velocity jump calculated from the solution within the critical layer.

Since most excitation devices tend to be two-dimensional, the initial oblique mode amplitudes should be much smaller than the initial plane wave amplitude. The initial nonlinear interaction will then be a secondary instability that leaves the plane wave growth rate unchanged while greatly enhancing the growth rate of the oblique modes. This might be termed the 'parametric resonance' stage. Previous studies

(Craik 1971; Smith & Stewart 1987; etc.) suggest that the plane-wave growth rate should be altered by the nonlinear interaction once the oblique-mode amplitudes become equal to that of the plane wave: which might be termed the 'fully coupled' (or 'fully interactive') stage. However, the present nonlinear interaction produces no critical-layer velocity jump at the fundamental frequency, which means that the two-dimensional mode continues to grow at its initial linear growth rate, even when the oblique modes become very large. This, in turn, allows these latter modes to exhibit faster-than-exponential growth (but not necessarily the very rapid exponential-of-an-exponential growth that would occur if the fully coupled terms were neglected in the Smith & Stewart 1987 analysis: see discussion in §7 below), even when they are much larger than the more slowly growing two-dimensional mode.

Of course, the oblique modes must eventually react back on the two-dimensional mode, but only when their (common) amplitude is of the order of the two-dimensional modal amplitude divided by the cube of the small streamwise wavenumber. The corresponding back-reaction term then turns out to be quartic in the oblique mode amplitudes rather than quadratic (as in the Raetz 1959; Craik 1971; and Smith & Stewart 1987 analyses). But even more importantly, the oblique modes are now large enough to interact nonlinearly within their common critical layer – producing a 'self-interaction' term, which does not appear in any of the previous analyses and which has a dramatic effect on the subsequent instability wave development. There is also a new mutual interaction term in the plane-wave amplitude equation which does not arise in previous analyses.

The self-interaction term causes the instability growth to increase beyond the faster-than-exponential growth of the parametric resonance stage and ultimately leads to a singularity at a finite downstream position. The local asymptotic expansions (which hold in the vicinity of the singularity) suggest that full (strong) nonlinearity will first come into play near the wall while the instability wave amplitude is still small and that the flow will then be governed by the three-dimensional, time-dependent, inviscid triple-deck equations in the next stage of evolution. However, the viscous terms were dropped before obtaining the final solutions†, and viscous effects within the critical layer could ultimately limit the instability wave growth and thereby eliminate the singularity (as in the related analysis of Goldstein & Leib 1989). Finally, we note that the significant qualitative differences between the present results and the previous zero-pressure-gradient solutions of Craik (1971), Smith & Stewart (1987), etc. provide additional justification for considering only the small-pressure-gradient case.

The overall plan of the paper is as follows. The problem is formulated in §2, where we show how the nonlinear critical-layer interaction gradually evolves from a resonant triad of linear small-growth-rate instability waves. The flow outside the critical layer is a linear three-dimensional perturbation about a steady two-dimensional boundary-layer flow subject to an externally imposed adverse pressure gradient. The classical long-wavelength Rayleigh's equation solution (in the form given by Miles 1962) is re-expanded in §3 to obtain the relevant solution in the main part of the boundary layer. In §4, we show that the linear Tollmien solution for the wall layer surrounding the critical layer (which always lies close to the wall in the long-wavelength small-growth-rate approximation being considered herein) can be

† The analytical results are exceedingly complex in the viscous case and it is best to solve the critical-layer equations numerically when viscosity is retained. This will be done in a subsequent paper.

matched onto the solution of §3. (A similar approach was used by Graebel 1966, Nield 1972, Smith & Bodonyi 1982, and Goldstein *et al.* 1987 to solve a related problem.) The analyses of these two sections are now quite routine, and we only briefly outline enough steps to make the paper self-contained.

The real complexity comes in when the critical layer is analysed in §5. The appropriate expansions are presented, and the solution that matches onto the upstream linear solution and onto the solution outside the critical layer is then found by integrating the first-order ordinary differential equation with respect to the streamwise coordinate. Matching with the external solution leads to a coupled set of nonlinear integro-differential equations for the amplitudes of the instability waves. While the algebraic manipulations turn out to be somewhat complex, we believe that the effort is more than justified by the relative simplicity of the final results ((5.50) and (5.51) below). Moreover, we have attempted to ease the burden to the reader by regulating the algebraic details to the appendices.

The relevant equations have to be solved subject to the upstream boundary conditions that their solutions match onto the linear instability waves far upstream (in terms of the appropriate scaled streamwise coordinate). Analytical solutions are obtained for the linear parametric resonance stage in Appendix E. However, the full nonlinear solutions have to be obtained numerically. These latter solutions always end in a singularity at a finite downstream position. The relevant local asymptotic solution is worked out in §6. The numerical results are discussed in §7.

2. Formulation

We suppose that the mean boundary-layer flow is two-dimensional and that the local Reynolds number R_Δ (based on the boundary-layer thickness Δ) is sufficiently large that the unsteady flow is nearly inviscid in the main part of the boundary layer and is nearly unaffected by boundary-layer growth over the region in which nonlinear interaction takes place. The mean flow velocity $U(y)$, which together with the complete flow velocity $\boldsymbol{u} = \{u, v, w\}$ is assumed to be normalized by the local free-stream velocity U_∞, then depends only on the transverse coordinate y to the required order of approximation. This coordinate, together with the streamwise and spanwise coordinates x and z, respectively, are normalized by Δ, the pressure p is normalized by the dynamic pressure ρU_∞^2, and the time t is normalized by Δ/U_∞. As indicated in §1, the upstream flow (in the region $x \to -\infty$) starts out as a triad of spatially growing linear instability waves: a single two-dimensional mode of (normalized) frequency ω and wavenumber α and two subharmonic oblique modes of frequency $\frac{1}{2}\omega$, streamwise wavenumber nearly equal to $\frac{1}{2}\alpha$ and spanwise wavenumbers $\pm\beta$.

Since the normalized mean pressure gradient μ (i.e. the local dimensional pressure gradient times the downstream distance divided by the dynamic pressure ρU_∞^2) is assumed to be small, the normalized complex wavenumber α must also be small and its imaginary part, which is controlled by μ, is then much smaller than its real part (Reid 1965; Smith & Bodonyi 1982; Goldstein *et al.* 1987). It follows that each of the three modes must have a critical layer at nearly the same transverse position, say y_c, where the real part of their nearly common phase velocity is equal to U. The smallness of μ also ensures that the mean boundary-layer velocity is given by the Blasius velocity U_B plus a small component U_p proportional to μ, and that

$$U_B \to U_0' y - \frac{U_0'^2}{2\times 4!} y^4 + \frac{11 U_0'^3}{4\times 7!} y^7 + \ldots, \qquad U_p \to \tfrac{1}{2}\mu y^2 + \ldots, \tag{2.1}$$

as $y \to 0$, where the wall is located at $y = 0$ and the constant U_0' denotes the scaled Blasius skin friction.

Arguments given, for example, in Goldstein *et al.* (1987, p. 328)† show that the three instability waves can only grow if

$$\mu - (\tfrac{1}{2}U_0' y_c)^2 > 0, \tag{2.2}$$

and the most rapidly growing modes correspond to the scaling

$$\mu = \sigma^2 \bar{\mu}, \tag{2.3}$$

$$\mathrm{Re}\,\alpha = \sigma\bar{\alpha} + O(\sigma^4), \tag{2.4}$$

$$\mathrm{Re}\,c_0 = \sigma\bar{c} + O(\sigma^4), \tag{2.5}$$

$$\beta = \sigma\bar{\beta}, \tag{2.6}$$

and

$$y_c = \sigma Y_c + O(\sigma^4), \tag{2.7}$$

where $\bar{\mu}$, $\bar{\alpha}$, $\bar{c}$, $\bar{\beta}$, and Y_c are order-one real constants (which depend on σ), and $\sigma^2 \ll 1$ characterizes the small pressure gradient. It could be more explicitly defined by setting $\bar{\mu} = 1$, but we retain $\bar{\mu}$ as a parameter to help clarify the role of the pressure gradient in our analysis. It now follows from (2.1) that

$$U = U_B + \sigma^2 \bar{U}_p \quad \text{for} \quad y = O(1), \tag{2.8}$$

where

$$\bar{U}_p \to \tfrac{1}{2}\bar{\mu} y^2 \quad \text{as} \quad y \to 0. \tag{2.9}$$

The unsteady flow outside the critical layer is still governed by linear dynamics to the required order of approximation, which means that the velocity field can be written as

$$u = U_B(y) + \sigma^2 \bar{U}_p(y) + \epsilon\,\mathrm{Re}\,A_0(x_1)\frac{\partial \Phi_0}{\partial y}(y, x_1, \sigma)\,\mathrm{e}^{\mathrm{i}X} + \delta[(2\cos Z)\,\mathrm{Re}\,A(x_1)\,\tilde{U}(y, x_1, \sigma)\,\mathrm{e}^{\mathrm{i}X/2} + \mathrm{Re}\,F_1^{(0)}(y, x_1\,\sigma)\,\mathrm{e}^{2\mathrm{i}Z}], \tag{2.10}$$

$$v = -\epsilon\,\mathrm{Re}\,\mathrm{i}\alpha A_0\,\Phi_0\,\mathrm{e}^{\mathrm{i}X} - \delta(2\cos Z)\,\mathrm{Re}\,\mathrm{i}\gamma A \Phi(y, x_1, \sigma)\,\mathrm{e}^{\mathrm{i}X/2} \tag{2.11}$$

and

$$w = \delta(2\sin Z)\,\mathrm{Re}\,\mathrm{i}A\tilde{W}(y, x_1, \sigma)\,\mathrm{e}^{\mathrm{i}X/2}, \tag{2.12}$$

where ϵ is a measure of the amplitude of the two-dimensional instability wave, δ is a measure of the (common) amplitude of the oblique modes,

$$\frac{(\gamma^2 - \beta^2)^{\frac{1}{2}}}{\gamma}\tilde{U} + \frac{\beta}{\gamma}\tilde{W} = \mathrm{D}\Phi, \tag{2.13}$$

$$\frac{\beta}{\gamma}\tilde{U} - \frac{(\gamma^2 - \beta^2)^{\frac{1}{2}}}{\gamma}\tilde{W} = \frac{\beta U'}{(\gamma^2 - \beta^2)^{\frac{1}{2}}}\frac{\Phi}{U - c}, \tag{2.14}$$

and we have put

$$x_1 = \sigma^4 x. \tag{2.15}$$

The quantities

$$X \equiv \sigma\bar{\alpha}(x - \sigma\bar{c}t) \tag{2.16}$$

and

$$Z \equiv \sigma\bar{\beta}z \tag{2.17}$$

are real to the required level of approximation, but we allow the modal amplitudes A and A_0 to be complex to account for possible wavenumber detuning. The X-

† Note that λ^2 should be deleted in their equation (2.5).

independent disturbance component in (2.10) is induced by nonlinear effects in the critical layer (Goldstein & Choi 1989). Φ and Φ_0 satisfy the Rayleigh's equations

$$(U-c)(\mathrm{D}^2-\gamma^2)\Phi - U''\Phi = 0, \tag{2.18}$$

$$(U-c_0)(\mathrm{D}^2-\alpha^2)\Phi_0 - U''\Phi_0 = 0, \tag{2.19}$$

and the complex wavenumbers γ and α and phase speeds c and c_0, respectively, are given to the required levels of approximation, by

$$\alpha = \sigma\bar{\alpha} + \sigma^4 A_0'/(\mathrm{i}A_0), \tag{2.20}$$

$$\gamma = \sigma\bar{\gamma} + \sigma^4\bar{\alpha}A'/(2\mathrm{i}\bar{\gamma}A), \tag{2.21}$$

$$c = \frac{\sigma\bar{c}}{1+(2\sigma^3/\mathrm{i}\bar{\alpha})(A'/A)}, \tag{2.22}$$

$$c_0 = \frac{\sigma\bar{c}}{1+(\sigma^3/\mathrm{i}\bar{\alpha})(A_0'/A_0)}, \tag{2.23}$$

where we have put

$$\bar{\gamma} \equiv [(\tfrac{1}{2}\bar{\alpha})^2 + \bar{\beta}^2]^{\frac{1}{2}}, \tag{2.24}$$

$$\mathrm{D} \equiv \partial/\partial y, \tag{2.25}$$

and the primes denote differentiation with respect to the relevant arguments.

Equations (2.13) and (2.14) can therefore be rewritten as

$$\tilde{U} = \cos\theta\left(\mathrm{D}\Phi + \tan^2\theta\frac{U'}{U-c}\Phi\right) + O(\sigma^3), \tag{2.26}$$

$$\tilde{W} = \sin\theta\left(\mathrm{D}\Phi - \frac{U'}{U-c}\Phi\right) + O(\sigma^3), \tag{2.27}$$

and

$$\tilde{U}\cos\theta + \tilde{\mathrm{W}}\sin\theta = \mathrm{D}\Phi - \frac{2\sigma^3}{\bar{\alpha}}\sin^2\theta\frac{U'}{U-c}\Phi\frac{A'}{\mathrm{i}A} + O(\sigma^4), \tag{2.28}$$

where

$$\theta \equiv \sin^{-1}(\beta/\bar{\gamma}) \tag{2.29}$$

is the propagation angle of the oblique modes.

Finally, Φ and Φ_0 must satisfy the boundary conditions

$$\Phi = \Phi_0 = 0 \quad \text{at} \quad y = 0, \tag{2.30}$$

for tangential flow near the wall.

3. Solutions in the main boundary layer

In this and the following sections we derive dispersion relations connecting the phase speed $\bar{c}$ and wavenumbers $\bar{\alpha}$, $\bar{\gamma}$, and $\bar{\beta}$ of the instability waves. They show that these latter quantities must have expansions of the form

$$\bar{\alpha} = \bar{\alpha}_0 + \sigma\bar{\alpha}_1 + \sigma^2\bar{\alpha}_2 + \sigma^3(\ln\sigma)\bar{\alpha}_{3L} + \sigma^3\bar{\alpha}_3 + \ldots \tag{3.1}$$

with similar expansions for $\bar{\gamma}$ and $\bar{\beta}$.

Since the analysis is now quite classical we include only enough steps to allow the reader to follow along without consulting numerous references.

First, suppose that $y = O(1)$. A number of investigators have obtained asymptotic expansions of the solution to (2.18) and (2.19) that are uniformly valid for $y = O(1)$ and $y \gg 1$ in the limit as $\gamma, \alpha \to 0$. The solutions to the present problems are most

easily obtained by re-expanding such a solution for small c or c_0. Since we need only know the logarithmic derivative of our solution, the most convenient solution turns out to be the one given by Miles (1962), obtained by transforming (2.18) or (2.19) into a Riccati equation. His result can be written as

$$\frac{\mathrm{D}\hat{\Phi}}{\hat{\Phi}} = \frac{U'}{U-\hat{c}} - \frac{1}{(U-\hat{c})^2\Omega^*} + O(\hat{\alpha}^5), \tag{3.2}$$

where

$$\Omega^* = \frac{1}{\hat{\alpha}(1-\hat{c})^2} + \Omega_0 + \hat{\alpha}\Omega_1 + \hat{\alpha}^2\Omega_2 + \ldots, \tag{3.3}$$

$$\Omega_0 = -\frac{1}{(1-\hat{c})^2}\int_y^\infty \left[\frac{(U-\hat{c})^2}{(1-\hat{c})^2} - \frac{(1-\hat{c})^2}{(U-\hat{c})^2}\right]\mathrm{d}y, \tag{3.4}$$

$$\Omega_1 = -\frac{2}{(1-\hat{c})^2}\int_y^\infty (U-\hat{c})^2\Omega_0\,\mathrm{d}y, \tag{3.5}$$

and

$$\Omega_2 = -\int_y^\infty (U-\hat{c})^2\left[\frac{2\Omega_1}{(1-\hat{c})^2} + \Omega_0^2\right]\mathrm{d}y, \tag{3.6}$$

where $\hat{\Phi}$ can denote either Φ or Φ_0, $\hat{c}$ can denote either c or c_0 and $\hat{\alpha}$ can denote either γ or α. A simple derivation is given in Reid (1965, p. 279). Matching is greatly simplified by using the classical 'inviscid function' (Lin 1955, p. 37)

$$\hat{W} \equiv \frac{\hat{c}\mathrm{D}\hat{\Phi}}{U'\hat{\Phi} - (U-\hat{c})\,\mathrm{D}\hat{\Phi}}. \tag{3.7}$$

Substituting (2.8), (2.20)–(2.23), and (3.2)–(3.6) into (3.7), expanding for small σ, and finally using (2.1) and (2.9), we obtain

$$W = \frac{\bar{c}U'}{\bar{\gamma}} + \sigma W^\dagger(y;\sigma,\bar{c},\bar{\gamma}) + \sigma^3\frac{\mathrm{i}\bar{c}U_0'}{\bar{\gamma}^2}\left(\cos\theta + \frac{1}{\cos\theta}\right)\frac{A'}{A} + O(\sigma^4), \tag{3.8}$$

$$W_0 = \frac{\bar{c}U'}{\bar{\alpha}} + \sigma W^\dagger(y;\sigma,\bar{c},\bar{\alpha}) + \sigma^3\frac{2\mathrm{i}\bar{c}U_0'}{\bar{\alpha}^2}\frac{A_0'}{A_0} + O(\sigma^4), \tag{3.9}$$

where $W^\dagger$ is purely real.

4. The Tollmien region (inviscid wall layer)

As was noted in a related context by Graebel (1966), Nield (1972), Smith & Bodonyi (1982), and Goldstein *et al.* (1987), the re-expansions (3.8) and (3.9) are invalid at distances from the wall of the order of the critical-layer distance $y_c = O(\sigma)$ since they correspond to the limiting process $\sigma \to 0$ with y fixed. The analyses of Nield (1972) and Graebel (1966) suggest that the scaled transverse coordinate

$$Y \equiv y/\sigma \tag{4.1}$$

be introduced directly into (2.18) and (2.19) before attempting to obtain the solution in this region. Inserting this along with (2.1), (2.8), (2.9), and (2.20)–(2.23) into (2.18) and (2.19), we find that the solutions which satisfy the boundary condition (2.30) are of the form

$$\Phi = \sigma(U_0' + \sigma a)\,Y + \sigma^4 F(Y,\phi) + \ldots, \tag{4.2}$$

$$\Phi_0 = \sigma(U_0' + \sigma a_0)\,Y + \sigma^4 F(Y,\phi_0) + \ldots, \tag{4.3}$$

where a and a_0 are order-one constants (which may depend on σ), and F satisfies

$$\frac{\partial^2 F}{\partial Y^2} = \bar{\mu}_c\left(1+\frac{Y_c}{Y-Y_c}\right) - \tfrac{1}{4}U_0'^2\, Y(Y_c+Y), \tag{4.4}$$

where

$$\bar{\mu}_c \equiv \bar{\mu} - (\tfrac{1}{2}U_0'\, Y_c)^2, \tag{4.5}$$

and we have used the fact that

$$\bar{c} = U_0'\, Y_c + O(\sigma), \tag{4.6}$$

where Y_c is defined by (2.7). Since (4.4) is singular at $Y = Y_c$, F can certainly be discontinuous across Y_c, and we denote by $F^{\pm}$ the solution above/below this point. Integrating (4.4) and imposing the boundary condition (2.30), we obtain

$$F^{\pm}(Y,\hat{\phi}) = f(Y) + \mathrm{i}\bar{\mu}_c\, Y_c[(Y-Y_c)\,\hat{\phi}^{\pm} + Y_c\,\hat{\phi}^{-}], \quad Y \gtrless Y_c, \tag{4.7}$$

where $f(Y) = \bar{\mu}_c\{\tfrac{1}{2}Y^2 + Y_c[(Y-Y_c)\ln|Y-Y_c| + Y_c\ln Y_c]\} - (U_0'^2/4!)\,Y^3(Y_c+\tfrac{1}{2}Y),$ (4.8)

and $\hat{\phi}^{\pm}$ denote either of the 'constants' of integration $\phi^{\pm}$ or $\phi_0^{\pm}$ which are, in general, complex functions of x_1.

As already anticipated, these solutions are most easily matched onto the solutions in the main boundary layer (where $y = O(1)$) by working with the inviscid functions W and W_0.

Inserting (2.1), (2.8), (2.9), (4.1)–(4.3), and (4.7) into (3.7) and re-expanding, we obtain

$$\hat{W} = \frac{U'}{U_0'} + \sigma^3\left[\frac{\bar{\mu}_c\, Y_c}{U_0'}\left(\ln\frac{Y-Y_c}{Y_c} - \mathrm{i}\Delta\hat{\phi}\right) - \tfrac{1}{8}U_0'\, Y_c\, Y(2Y_c+Y)\right] + O(\sigma^4) \tag{4.9}$$

for $Y > Y_c$, where $\Delta\hat{\phi}$ denotes either $\phi^- - \phi^+$ or $\phi_0^- - \phi_0^+$. Matching with (3.8) and (3.9) shows that

$$\bar{\gamma} = \bar{\alpha} + 2\sigma^3\kappa_1 + O(\sigma^4), \tag{4.10}$$

$$U_0'\,\bar{c}/\bar{\alpha} = 1 + O(\sigma), \tag{4.11}$$

$$\left(\cos\theta + \frac{1}{\cos\theta}\right)\frac{A'}{A} = -\frac{\bar{\gamma}^2\bar{\mu}_c}{\bar{c}U_0'^2}\, Y_c\,\Delta\phi, \tag{4.12}$$

and

$$\frac{A_0'}{A_0} = -\frac{\bar{\alpha}^2\bar{\mu}_c}{2\bar{c}U_0'^2}\, Y_c\,\Delta\phi_0 + \mathrm{i}\kappa_1, \tag{4.13}$$

where κ_1 is the initial wavenumber 'detuning' which can be chosen arbitrarily as an initial condition.

Equations (4.10) and (4.11) are dispersion relations which determine $\bar{\alpha}$ and $\bar{\gamma}$ in terms of $\bar{c}$ (or in terms of the scaled Strouhal number $\bar{\alpha}\bar{c}$). Since their coefficients are all real they are consistent with our original assertion that $\bar{\alpha}$ and $\bar{c}$ are real quantities. They show that $\bar{\alpha}$, $\bar{\beta}$, $\bar{\gamma}$ and $\bar{c}$ possess power-series expansions (3.1). In fact it follows from (2.24) and (4.10) that

$$\bar{\beta} = \tfrac{1}{2}\sqrt{3}\bar{\alpha} + (4/\sqrt{3})\,\sigma^3\kappa_1 + O(\sigma^4), \tag{4.14}$$

which shows $\bar{\beta}$ and $\bar{\alpha}$ satisfy the usual long-wavelength small-growth-rate resonance condition (see also Smith & Stewart 1987) to within the order of the detuning. Equation (4.11) shows that $\bar{c}_0$ and $\bar{\alpha}_0$ satisfy the usual long-wavelength small-growth-rate dispersion relation

$$\bar{c}_0 = \bar{\alpha}_0/U_0'. \tag{4.15}$$

Equations (4.12) and (4.13) roughly correspond to the imaginary parts of the dispersion relations; they relate the (slow) growth rates of the instability waves A'/A and A_0'/A_0 to the phase jumps $\Delta\phi$ and $\Delta\phi_0$ across the critical layer. To determine these latter quantities, it is necessary to consider the flow in the critical layer.

Equations (2.10)–(2.12), (2.26)–(2.29), (4.2), (4.3), and (4.7) show that

$$u = \sigma U_0' Y + \sigma^4 \tfrac{1}{2} Y^2 \left(\bar{\mu} - \frac{U_0'^2}{4!} Y^2\right) + \epsilon \,\mathrm{Re}\left[U_0' + \sigma a_0 + \sigma^3 \left(\frac{\mathrm{d}f}{\mathrm{d}Y} + \mathrm{i}\bar{\mu}_c Y_c \phi_0^{\pm}\right)\right] A_0 \,\mathrm{e}^{\mathrm{i}X}$$

$$+ 2\delta(\sec\theta \cos Z)\,\mathrm{Re}\left\{(U_0' + \sigma a)(1 + \zeta \sin^2\theta) + \sigma^3 \frac{U_0' \zeta}{\bar{c}} \sin^2\theta \left[f + \tfrac{1}{2}\bar{\mu} Y^2 (1-\zeta)\right.\right.$$

$$\left. - \frac{U_0'^2 Y^4}{2 \times 4!}(3-\zeta) + \frac{\bar{c}}{U_0' \zeta \tan^2\theta} \frac{\mathrm{d}f}{\mathrm{d}Y} - \frac{\bar{c} A'}{\bar{\gamma} \mathrm{i} A}\left(\cos\theta + \frac{U_0'^2 Y^2}{\bar{c}^2} \frac{\zeta}{\cos\theta}\right)\right.$$

$$\left.\left. + \frac{\mathrm{i}\bar{c}\bar{\mu}_c Y_c}{U_0'}\left(\phi^- + \frac{1}{\zeta \sin^2\theta}\phi^{\pm}\right)\right]\right\} A \,\mathrm{e}^{\mathrm{i}X/2} + \delta \,\mathrm{Re} f_1^{(0)}(Y_{c\pm}, x_1)\,\mathrm{e}^{2\mathrm{i}Z} + \ldots, \tag{4.16}$$

$$v = -\sigma^2 U_0' Y[\epsilon \,\mathrm{Re}\,\mathrm{i}\bar{\alpha} A_0 \,\mathrm{e}^{\mathrm{i}X} + \delta \,\mathrm{Re}\, 2\mathrm{i}\bar{\gamma}(\cos Z) A \,\mathrm{e}^{\mathrm{i}X/2}] + \ldots, \tag{4.17}$$

$$w = -2\delta(\sin\theta \sin Z)\,\mathrm{Re}\, U_0' \zeta \mathrm{i} A \,\mathrm{e}^{\mathrm{i}X/2} + \ldots, \tag{4.18}$$

$$p = P + \sigma\bar{c} U_0'[\epsilon \,\mathrm{Re}\, A_0 \,\mathrm{e}^{\mathrm{i}X} + 2\delta(\cos\theta \cos Z)\,\mathrm{Re}\, A \,\mathrm{e}^{\mathrm{i}X/2}] + \ldots, \tag{4.19}$$

where $f_1^{(0)}$ is the wall-layer expansion corresponding to $F_1^{(0)}$ in (2.10), we have put

$$\zeta \equiv \bar{c}/(U_0' Y - \bar{c}), \tag{4.20}$$

and P denotes the more-or-less constant mean pressure at the critical level. These clearly become singular at the critical level $Y = Y_c$. The solution therefore has to be rescaled in this region.

5. The critical level

The thickness of the linear, small-growth-rate critical layer is of the same order as the growth rate, i.e. $O(\sigma^4)$ in the present case. The appropriate transverse coordinate in this region is therefore

$$\bar{\eta} = (Y - Y_c)/\sigma^3 = (y - y_c)/\sigma^4. \tag{5.1}$$

Viscous effects will enter the critical-layer momentum equation while making only relatively insignificant modifications in the external flow (see (5.34) below) when the Benney–Bergeron (1969) parameter

$$\lambda \equiv 1/(R_A \sigma^{13}) \tag{5.2}$$

is order one. The solutions in this region should depend on x and t only through the scaled variables (2.15) and (2.16). The governing equations should therefore be expressed in terms of the scaled variables x_1, X, Z, and $\bar{\eta}$ to obtain

$$\bar{\mathrm{D}}\boldsymbol{u} = -\{\bar{\alpha} p_X + \sigma^3 p_{x_1}, \sigma^{-10} p_{\bar{\eta}}, \bar{\beta} p_Z\}, \tag{5.3}$$

and

$$\bar{\alpha} u_X + \bar{v}_{\bar{\eta}} + \bar{\beta} w_Z + \sigma^3 u_{x_1} = 0, \tag{5.4}$$

where we have put

$$\bar{\mathrm{D}} \equiv \bar{\alpha}(u - \sigma\bar{c})\frac{\partial}{\partial X} + \bar{v}\frac{\partial}{\partial\bar{\eta}} + \bar{\beta} w \frac{\partial}{\partial Z} + \sigma^3 u \frac{\partial}{\partial x_1} - \sigma^4 \lambda \frac{\partial^2}{\partial\bar{\eta}^2}, \tag{5.5}$$

$$v = \sigma^5 \bar{v}, \tag{5.6}$$

and
$$\boldsymbol{u} \equiv \{u, \bar{v}, w\}. \tag{5.7}$$

The nonlinear terms in the critical-layer solution will balance the velocity jump when
$$\epsilon = \sigma^{13}. \tag{5.8}$$
As indicated in the introduction the self-interaction between the oblique modes produces a non-zero velocity jump across the critical layer when their characteristic amplitude δ is $O(\sigma^{10})$. This will just balance the corresponding linear growth rate term if we take
$$\epsilon = \sigma^3\delta. \tag{5.9}$$
Introducing (5.1), (5.8), and (5.9) into (4.16) to (4.19) and re-expanding the result for small $\bar{\eta}$ shows that the critical-layer solution should be of the form
$$u - \sigma\bar{c} = \sigma^4 U_0'\,\bar{\eta} + \sigma^7 u^{(1)} + \sigma^{10}u^{(2)} + \sigma^{13}u^{(3)} + \sigma^{16}u^{(4)} + \ldots, \tag{5.10}$$
$$\bar{v} = -\sigma^7 2\bar{\gamma}U_0'\,Y_c(\cos Z)\,\mathrm{Re}\,\mathrm{i}A\,\mathrm{e}^{\mathrm{i}X/2} + \sigma^{10}\bar{v}^{(2)} + \sigma^{13}\bar{v}^{(3)} + \sigma^{16}\bar{v}^{(4)} + \ldots, \tag{5.11}$$
$$w = \sigma^7 w^{(1)} + \sigma^{10}w^{(2)} + \sigma^{13}w^{(3)} + \sigma^{16}w^{(4)} + \ldots, \tag{5.12}$$
and
$$p = P + \sigma^{11}2\bar{c}U_0'(\cos\theta\cos Z)\,\mathrm{Re}\,A\,\mathrm{e}^{\mathrm{i}X/2} + \sigma^{14}p^{(2)} + \sigma^{17}p^{(3)} + \sigma^{20}p^{(4)} + \ldots, \tag{5.13}$$
where the $u^{(l)}$, $\bar{v}^{(l)}$, $w^{(l)}$, and $p^{(l)}$ are functions only of x_1, X, Z, and $\bar{\eta}$.

Substituting the expansions (5.10)–(5.13) into (5.3)–(5.7) we find that
$$\mathscr{L}u^{(1)} = (2U_0'\bar{c}/\bar{\gamma})\,\bar{\beta}^2(\cos Z)\,\mathrm{Re}\,\mathrm{i}A\,\mathrm{e}^{\mathrm{i}X/2}, \tag{5.14}$$
$$\mathscr{L}w^{(1)} = (U_0'\bar{c}/\bar{\gamma})\,\bar{\alpha}\bar{\beta}(\sin Z)\,\mathrm{Re}\,A\,\mathrm{e}^{\mathrm{i}X/2}, \tag{5.15}$$
$$\mathscr{L}u_{\bar{\eta}}^{(l)} = G^{(l)} \quad \text{for} \quad l = 2, 3 \text{ and } 4, \tag{5.16}$$
$$\mathscr{L}w^{(l)} = H^{(l)} \quad \text{for} \quad l = 2 \text{ and } 3, \tag{5.17}$$
$$\bar{\alpha}u_X^{(1)} + \bar{\beta}w_Z^{(1)} = 0, \tag{5.18}$$
$$\bar{\alpha}u_X^{(l)} + u_{x_1}^{(l-1)} + \bar{v}_{\bar{\eta}}^{(l)} + \bar{\beta}w_Z^{(l)} = 0 \quad \text{for} \quad l = 2 \text{ and } 3, \tag{5.19}$$
and
$$p_{\bar{\eta}}^{(l)} = 0 \quad \text{for} \quad l = 2 \text{ and } 3, \tag{5.20}$$
where $G^{(l)}$ and $H^{(l)}$ are functions of lower-order solutions and defined in Appendix A, and we have put
$$\mathscr{L} \equiv \bar{c}\,\partial/\partial x_1 + \bar{\alpha}U_0'\,\bar{\eta}\,\partial/\partial X - \lambda\,\partial^2/\partial\bar{\eta}^2. \tag{5.21}$$

We must now solve (5.14)–(5.20) subject to the transverse boundary condition that they match onto the outer solution (4.16)–(4.19), but before this is done it is convenient to introduce the following normalized variables:
$$\tilde{x} = U_0'^{\frac{1}{2}}\bar{\alpha}x_1 - x_0, \tag{5.22}$$
$$\eta = \bar{\eta}/\bar{c}, \tag{5.23}$$
and
$$\bar{\lambda} = 2\lambda/(\bar{\alpha}U_0'\bar{c}^3), \tag{5.24}$$
where x_0 is a coordinate origin shift, to be chosen subsequently (see (5.59) below).

It is clear from (5.14) and (5.15) that the relevant lowest-order solutions are given by
$$u^{(1)} = \bar{c}\bar{\mu}_c^{\dagger}\,Y_c\,\eta + 2(\tan\theta\cos Z)\,\mathrm{Re}\,\mathrm{i}Q^{(1)}(\eta, \tilde{x})\,\mathrm{e}^{\mathrm{i}X/2}, \tag{5.25}$$
$$w^{(1)} = 2(\sin Z)\,\mathrm{Re}\,Q^{(1)}(\eta, \tilde{x})\,\mathrm{e}^{\mathrm{i}X/2}, \tag{5.26}$$
where $Q^{(1)}$ satisfies
$$\mathrm{L}_1\,Q^{(1)} = (\sin\theta)\,A, \tag{5.27}$$
subject to the transverse boundary condition
$$Q^{(1)} \sim 1/\eta \quad \text{as} \quad \eta \to \pm\infty, \tag{5.28}$$
we have put
$$\mathrm{L}_n \equiv \partial/\partial\tilde{x} + \mathrm{i}n\eta - \bar{\lambda}\,\partial^2/\partial\eta^2 \quad \text{for} \quad n = 0, 1, 2, \ldots, \tag{5.29}$$

and
$$\bar{\mu}_c^{\dagger} \equiv \bar{\mu} - \tfrac{1}{3}(\tfrac{1}{2}U_0' Y_c)^2. \tag{5.30}$$

Equations (5.16) and (5.17) clearly possess solutions of the form

$$u_\eta^{(l)} = Q_M^{(l)} + \mathrm{Re} \sum_{n=0}^{l} \sum_{m=-l}^{l} Q_{n,m}^{(l)}(\eta, \tilde{x}) \exp[\mathrm{i}(\tfrac{1}{2}nX + mZ)] \quad \text{for} \quad l = 2, 3 \text{ and } 4, \tag{5.31}$$

$$w^{(l)} = \mathrm{Re} \sum_{n=0}^{l} \sum_{m=-l}^{l} W_{n,m}^{(l)}(\eta, \tilde{x}) \exp[\mathrm{i}(\tfrac{1}{2}nX + mZ)] \quad \textit{for} \quad l = 2, 3 \text{ and } 4, \tag{5.32}$$

where
$$Q_M^{(2)} = (\bar{\mu} - \tfrac{1}{4}\bar{c}^2)\,\bar{c}^2\eta + \ldots, \tag{5.33}$$

$$Q_M^{(3)} = -\tfrac{1}{4}\bar{c}^6 U_0'^2 Y_c\,\eta^2 - \tfrac{1}{2}\bar{\lambda}\bar{c}^4 U_0'(\tilde{x} + x_0) + \ldots, \tag{5.34}$$

the passive linear term in $\tilde{x}$ is included in (5.34) to match a slight viscous correction that enters the external solution (4.16) due to the slow viscous spreading of the mean flow, and the dots in (5.33) and (5.34) represent the terms which are independent of $\tilde{x}$ and are omitted because they do not play any active role in our matching procedure. We have included $Q_M^{(l)}$ in (5.31) to ensure that

$$Q_{n,m}^{(l)}, Q_{2,0}^{(4)} \to 0 \quad \text{as} \quad \eta \to \pm\infty \quad \text{for} \quad l = 2 \text{ and } 3, \tag{5.35}$$

and $W_{n,m}^{(l)}$ must satisfy the transverse boundary condition

$$W_{n,m}^{(2)}, W_{3,1}^{(3)} \to 0 \quad \text{and} \quad W_{1,1\eta}^{(3)} \to 0 \quad \text{as} \quad \eta \to \pm\infty. \tag{5.36}$$

Substituting (5.31) and (5.32) along with (5.25) and (5.26) into (5.16) and (5.17) shows that

$$\mathrm{L}_n Q_{n,m}^{(l)} = \mathscr{G}_{n,m}^{(l)} \quad \text{for} \quad l = 2, 3 \text{ and } 4, \tag{5.37}$$

$$\mathrm{L}_n W_{n,m}^{(l)} = \mathscr{H}_{n,m}^{(l)} \quad \text{for} \quad l = 2 \text{ and } 3, \tag{5.38}$$

and differentiating (5.38) with respect to η, combining with (5.37) for $l = 3$ and $n = m = 1$ we obtain after considerable manipulation

$$\mathrm{L}_1 q_{1,1}^{(3)} = \mathscr{R}_{1,1}^{(3)}, \tag{5.39}$$

where we have put

$$q_{1,1}^{(3)} \equiv Q_{1,1}^{(3)} + \tan\theta[W_{1,1}^{(3)} + \mathrm{i}U_0'(W_{1,1}^{(2)} + U_0' Q_{\tilde{x}}^{(1)})_{\tilde{x}}]_\eta, \tag{5.40}$$

and $\mathscr{G}_{n,m}^{(l)}$, $\mathscr{H}_{n,m}^{(l)}$, and $\mathscr{R}_{1,1}^{(3)}$ are defined in Appendix B.

It now follows from (4.12), (4.13), (5.10), (5.31), and (5.40) that these solutions must satisfy

$$\int_{-\infty}^{\infty} q_{1,1}^{(3)}\,\mathrm{d}\eta = \mathrm{i}\frac{\bar{c}U_0'^3}{\bar{\gamma}}\left(\cos\theta + \frac{1}{\cos\theta}\right)A', \tag{5.41}$$

$$\int_{-\infty}^{\infty} Q_{2,0}^{(4)}\,\mathrm{d}\eta = \mathrm{i}\frac{\bar{c}U_0'^3}{\bar{\alpha}}\left(A_0' - \mathrm{i}\frac{2}{\bar{\alpha}U_0'}\kappa_1 A_0\right), \tag{5.42}$$

in order to match onto the discontinuous $O(\delta\sigma^3) = O(\sigma^{13})$ and $O(\epsilon\sigma^3) = O(\sigma^{16})$ terms in (4.16) for the oblique and two-dimensional modes respectively. These equations ultimately determine the unknown instability wave amplitudes A and A_0. They arise from the requirement that the change in the fundamental and subharmonic components of the velocity fluctuation across the critical layer as calculated from the external solutions are the same as when they are calculated from the internal solutions.

The latter solutions can be found by solving (5.27), substituting the solution in (5.37) to (5.39) and then solving the result. For simplicity we consider only the

inviscid case. The relevant derivations are summarized in Appendix C. Substituting these solutions into (5.41) and (5.42) now shows that the amplitudes A and A_0 satisfy integro-differential equations. Upon noting that (see (2.29), (4.10), (4.14), and (4.15))

$$\bar{\alpha} = \bar{\gamma}, \quad \cos\theta = \tfrac{1}{2}, \quad \bar{c} = \bar{\alpha}/U_0' = U_0' Y_c \tag{5.43}$$

to the order of approximation of the analysis, and putting

$$\tilde{X} = X - X_0, \tag{5.44}$$

$$\bar{x} = \kappa_0 \tilde{x}, \tag{5.45}$$

$$\tilde{A} = (M^{\frac{1}{3}}/\bar{\alpha}^{\frac{1}{3}}\kappa_0^3) A \, e^{iX_0/2}, \tag{5.46}$$

$$\tilde{A}_0 = (M/\kappa_0^4) A_0 \, e^{iX_0}, \tag{5.47}$$

where X_0 is the coordinate origin shift, and

$$\kappa_0 = (\pi Y_c/U_0'^2)\bar{\mu}_c, \tag{5.48}$$

$$M = 6\pi/(U_0'^3 \bar{c}), \tag{5.49}$$

we find that the amplitude equations can be written as

$$\frac{d\tilde{A}}{d\bar{x}} = \tfrac{4}{5}\tilde{A} + \tfrac{2}{5}i \int_{-\infty}^{\bar{x}} (\bar{x}-x_1)^2 \tilde{A}_0(x_1) \tilde{A}^*(2x_1 - \bar{x}) \, dx_1$$
$$+ i \int_{-\infty}^{\bar{x}} \int_{-\infty}^{x_1} K_1(\bar{x}\,|\,x_1, x_2) \tilde{A}(x_1) \tilde{A}(x_2) \tilde{A}^*(x_1 + x_2 - \bar{x}) \, dx_2 \, dx_1, \tag{5.50}$$

$$\frac{d\tilde{A}_0}{d\bar{x}} = (1 + i\tilde{\kappa}_1)\tilde{A}_0 - i \int_{-\infty}^{\bar{x}} \int_{-\infty}^{x_1} [2(\bar{x}-x_1)^3 \tilde{A}_0(x_1) \tilde{A}(x_2) \tilde{A}^*(2x_1 + x_2 - 2\bar{x})$$
$$+ K_2(\bar{x}\,|\,x_1, x_2) \tilde{A}(x_1) \tilde{A}_0(x_2) \tilde{A}^*(x_1 + 2x_2 - 2\bar{x})] \, dx_2 \, dx_1$$
$$+ i \int_{-\infty}^{\bar{x}} \int_{-\infty}^{x_1} \int_{-\infty}^{x_2} K_3(\bar{x}\,|\,x_1, x_2, x_3) \tilde{A}(x_1) \tilde{A}(x_2) \tilde{A}(x_3) \tilde{A}^*(x_1 + x_2 + x_3 - 2\bar{x}) \, dx_3 \, dx_2 \, dx_1, \tag{5.51}$$

where the asterisks denote the complex conjugates,

$$K_1 = \tfrac{1}{10}(\bar{x}-x_1)[2(\bar{x}-x_1)^2 - (\bar{x}-x_1)(\bar{x}-x_2) + 3(\bar{x}-x_2)^2], \tag{5.52}$$

$$K_2 = (\bar{x}-x_1)(\bar{x}-x_2)(2\bar{x}-x_1-x_2), \tag{5.53}$$

$$K_3 = \tfrac{1}{4}(\bar{x}-x_1)[(\bar{x}+x_1+x_2-3x_3)(\bar{x}-x_3)(\bar{x}-2x_1+x_2)$$
$$- (\bar{x}+x_1-2x_2)\{(\bar{x}+x_1-2x_2)^2 - 3(\bar{x}-x_2)^2\}], \tag{5.54}$$

and

$$\tilde{\kappa}_1 = (2/\bar{\alpha}U_0')(\kappa_1/\kappa_0). \tag{5.55}$$

Equations (5.50) and (5.51) are the final results which determine the amplitudes of the instability waves. They must be solved subject to the upstream boundary conditions in order to match onto the linear solution far upstream in the flow:

$$\tilde{A} \to a^{(0)} e^{4\bar{x}/5} \quad \text{as} \quad \bar{x} \to -\infty, \tag{5.56}$$

$$\tilde{A}_0 \to e^{(1+i\tilde{\kappa}_1)\bar{x}} \quad \text{as} \quad \bar{x} \to -\infty, \tag{5.57}$$

where

$$a^{(0)} = \frac{1}{\bar{\alpha}^{\frac{1}{3}}\kappa_0} \frac{A^{(0)}}{(A_0^{(0)})^{\frac{1}{3}}} \left(\frac{M}{\kappa_0^4}|A_0^{(0)}|\right)^{-3/10 + i\tilde{\kappa}_1/2}, \tag{5.58}$$

and $A^{(0)}$ and $A_0^{(0)}$ are the (complex) scaled initial instability wave amplitudes. The origin shifts x_0 and X_0 in (5.22) and (5.44) are chosen to satisfy

$$(M/\kappa_0^4) A_0^{(0)} \exp[\kappa_0(1 + i\tilde{\kappa}_1) x_0] \exp[iX_0] = 1. \tag{5.59}$$

The interpretation of the various terms in (5.50) and (5.51) will be deferred to §7, where the numerical solutions are also discussed.

6. Asymptotic solution of the amplitude equation

We first note that the solutions always develop a singularity at some finite value of $\bar{x}$, say $\bar{x}_s$. In this section we determine the asymptotic form of the solution as $\bar{x} \to \bar{x}_s$. To this end we substitute

$$\tilde{A} = b/(\bar{x}_s - \bar{x})^{3+i\psi}, \tag{6.1}$$

and

$$\tilde{A}_0 = b_0/(\bar{x}_s - \bar{x})^{4+2i\psi}, \tag{6.2}$$

where $\bar{x}_s$ and ψ are real constants and b and b_0 are complex constants, into the integrals of (5.50) and (5.51) and change the integration variables from $\bar{x}_n$ for $n = 1, 2$, and 3 to $(\bar{x}_s - x_n)/(\bar{x}_s - \bar{x})$ to show that

$$\frac{2}{5}\int_{-\infty}^{\bar{x}} (\bar{x}-x_1)^2 \tilde{A}_0(x_1)\tilde{A}^*(2x_1-\bar{x})\,dx_1 = \frac{b_0 b^*}{(\bar{x}_s-\bar{x})^{4+i\psi}} D_1(\psi), \tag{6.3}$$

$$\int_{-\infty}^{\bar{x}}\int_{-\infty}^{x_1} K_1(\bar{x}\,|\,x_1,x_2)\tilde{A}(x_1)\tilde{A}(x_2)\tilde{A}^*(x_1+x_2-\bar{x})\,dx_2\,dx_1 = \frac{b|b|^2}{(\bar{x}_s-\bar{x})^{4+i\psi}} D_2(\psi), \tag{6.4}$$

$$\int_{-\infty}^{\bar{x}}\int_{-\infty}^{x_1} [2(\bar{x}-x_1)^3 \tilde{A}_0(x_1)\tilde{A}(x_2)\tilde{A}^*(2x_1+x_2-2\bar{x}) + K_2(\bar{x}\,|\,x_1,x_2)\tilde{A}(x_1)\tilde{A}_0(x_2)$$

$$\times \tilde{A}^*(x_1+2x_2-2\bar{x})]\,dx_2\,dx_1 = \frac{b_0|b|^2}{(\bar{x}_s-\bar{x})^{5+2i\psi}} D_3(\psi), \tag{6.5}$$

$$\int_{-\infty}^{\bar{x}}\int_{-\infty}^{x_1}\int_{-\infty}^{x_2} K_3(\bar{x}\,|\,x_1,x_2,x_3)\tilde{A}(x_1)\tilde{A}(x_2)\tilde{A}(x_3)\tilde{A}^*(x_1+x_2+x_3-2\bar{x})\,dx_3\,dx_2\,dx_1$$

$$= \frac{b^2|b|^2}{(\bar{x}_s-\bar{x})^{5+2i\psi}} D_4(\psi), \tag{6.6}$$

where the D_n are defined in Appendix D.

$\tilde{A}_{\bar{x}}$ and $\tilde{A}_{0\bar{x}}$ become large compared with $\tilde{A}$ and $\tilde{A}_0$ as $\bar{x} \to \bar{x}_s$, and the left-hand sides of (5.50) and (5.51) are balanced by the integral terms on the right-hand sides. Substituting (6.1) and (6.2) into the left-hand sides shows that the terms will balance when

$$\frac{3+i\psi}{|b|^2} = i\left(\frac{b_0}{b^2}D_1(\psi) + D_2(\psi)\right), \tag{6.7}$$

$$\frac{4+2i\psi}{|b|^2} = i\left(-D_3(\psi) + \frac{b^2}{b_0}D_4(\psi)\right), \tag{6.8}$$

which can be solved to determine ψ, $|b|$, $|b_0|$, and the argument of b^2/b_0. Notice that the individual arguments of b and b_0 are, at this stage, indeterminate.

7. Discussion and results

The amplitude equations (5.50) and (5.51), together with the upstream boundary conditions (5.56) and (5.57), are the main results of this paper. They only apply to the inviscid case. However, they can, in principle, be modified to include viscosity, but the resulting formulae would then be exceedingly complex. It would therefore be better to account for viscous effects by numerically solving (5.27) and (5.37)–(5.39) subject to the jump conditions (5.41) and (5.42). This will be done in a subsequent

paper. Here, we merely note that the resulting solutions will not be uniformly valid as the frequency ω^* goes to zero because the viscous Stokes layer at the wall eventually contributes term $U_0'^2\bar{c}^3/[2R_\Delta(\omega^*\Delta/U_\infty)^5]^{\frac{1}{2}}$ to the scaled linear growth rate (5.48) when ω^* becomes sufficiently small. However, the viscous solution can be made uniformly valid for all frequencies by replacing κ_0 with $\kappa_0+U_0'^2\bar{c}^3/[2R_\Delta(\omega^*\Delta/U_\infty)^5]^{\frac{1}{2}}$.

The system (5.50), (5.51), (5.56), and (5.57) contains three independently controllable parameters: $\tilde{\kappa}_1$, which accounts for the effect of initial wavenumber detuning and extends the analysis to the off-resonance case; $\arg(a^{(0)})$, which accounts for the initial phase difference between the oblique modes and the plane wave; and $|a^{(0)}|$, which accounts for the initial amplitude ratio of the oblique modes relative to the plane wave. The effect of each of these parameters is discussed below, but first we note that (5.50) and (5.51) are integro-differential equations (of the type considered by Hickernell 1984; Goldstein & Leib 1989; and Leib 1991 in a slightly different context; and Goldstein & Choi 1989 in a more closely related context) rather than the usual ordinary differential equations of the type first considered by Stuart (1960), Watson (1960), and Landau & Lifshitz (1987, §26) in the plane wave context, and by Craik (1971), Smith & Stewart (1987), and others in the resonant-triad context. The reason for this difference is that the nonlinear interactions now occur entirely within the non-equilibrium-type critical layer rather than in the external flow. This causes a gradual phase shifting between the different modes that can interact within that critical layer to produce a kind of upstream history effect, which results in the integral terms appearing on the right-hand sides of (5.50) and (5.51).

It is worth noting that the present paper is the first to consider coupled amplitude equations of this type and that the behaviour of the coupling terms is therefore of special interest. We now go through these equations term by term. The first terms on the right-hand sides are just the linear growth rate terms and are all that remain when the amplitudes become sufficiently small. (Note the initial wavenumber detuning factor that appears in the linear term of (5.51).) The second term on the right-hand side of (5.50) is a 'mutual interaction' term that accounts for the effect of the plane wave on the oblique mode. The non-integral analogue of this term is also present in the resonant-triad analyses of Craik (1971) and Smith & Stewart (1987), and the scaling (5.9) suggests that it will be the dominant nonlinear term in both (5.50) and (5.51) whenever

$$O(\delta) < O(\epsilon/\sigma^3), \tag{7.1}$$

i.e. whenever the oblique-mode amplitude is small compared with the two-dimensional wave amplitude divided by the cube of the (small) streamwise wavenumber scale. Equations (2.11), (2.20), and (5.8) show that this stage first occurs when the cross-flow velocity fluctuation of the plane wave is of order σ^{14} in the main part of the boundary layer – with the linear instability wave growth rate being of $O(\sigma^4) = O$ (adverse pressure gradient)^2. The nonlinear interaction therefore occurs when the two-dimensional instability amplitude gets to be of the order of the adverse pressure gradient to the seventh power (or, equivalently, the linear instability wave growth rate to the power $\frac{7}{2}$). This is in contrast to the Raetz (1959)–Craik (1971) formulation in which the interaction occurs when the amplitude is of the order of the linear growth rate.

This stage might be termed the 'parametric resonance' or 'secondary instability' stage, since the plane wave continues to exhibit linear growth, and the oblique mode is then determined by a linear equation with known coefficients. The solution to this equation is given in Appendix E. It shows that the oblique-mode instability wave

amplitude $\tilde{A}$ can itself be represented by a superposition of modes, each of which exhibits exponential growth. This solution also shows that $\tilde{A}$ tends to be dominated by the lower-order modes at small values of $\bar{x}$, but that the higher modes rapidly come into play and the 'infinite tail' of the series eventually determines the behaviour of the solution at large values of $\bar{x}$. In which case, (E 26) shows that $\tilde{A}$ behaves like

$$\tilde{A} \propto e^{4\bar{x}/5} e^{-3\bar{x}/5} \exp\left[\int_{-\infty}^{\bar{x}} (\bar{A}_0/10)^{\frac{1}{4}} d\bar{x}\right] \quad \text{as} \quad \bar{x} \to \infty, \tag{7.2}$$

where $\tilde{A}_0$ is given by (E 2).

The first factor is the linear growth term, so that the next two factors represent a net augmentation of the growth above the linear growth. The last factor shows that exponential-of-an-exponential growth does occur in this limit. The Smith & Stewart (1987) solution will also exhibit faster than exponential growth when the back-reaction terms are neglected in their amplitude equation (i.e. their (3.1*b*) and (3.1*c*)), but the detailed behaviour is quite different from theirs (e.g. our growth rate is proportional to $\tilde{A}_0^{\frac{1}{4}}$ while theirs is proportional to $\tilde{A}_0$).

When $\tilde{A}$ is sufficiently small, the plane wave can become fully nonlinear before it is affected by the oblique modes. This will occur when $\tilde{A}_0$ becomes $O(\sigma^{-6})$ before back reaction can occur. $\tilde{A}$ will then evolve on the lengthscale $\bar{x}/\sigma^{\frac{3}{4}}$, the oblique-wave critical-layer thickness will then be much larger than that of the plane wave, and the oblique mode amplitude will still be determined by (an appropriately scaled version of) (E 1) but with $\tilde{A}_0$ factored out of the integral and the first (i.e. linear growth) term omitted from the right-hand side. The relevant solution is still given by (7.2) to within slowly varying amplitude function, but with $\tilde{A}_0$ now given by the nonlinear critical-layer solution of Goldstein *et al.* (1987) rather than by (E 2). Details will be given in a forthcoming paper.

However, the limit (7.2) is often never reached because (5.50) and (5.51) become fully interactive before it can occur. We term this latter stage the 'fully coupled' or 'fully interactive' stage. Equations (5.8) and (5.9) show that it occurs when the oblique-mode amplitudes become of the order of the instability wave growth rate to the power $\frac{5}{2}$. More importantly, however, the back-reaction term, i.e. the final term on the right-hand side of (5.51) is now quartic in the instability-wave amplitudes, rather than quadratic as in the analyses of Craik (1971), Smith & Stewart (1987), etc. There is also a mutual interaction term which appears on the right-hand side of (5.51) but does not occur in any previous resonant-triad analysis.

However, the most significant new effect is that the oblique modes can now interact with themselves to produce the cubic 'self-interaction' term on the right-hand side of (5.50) once their amplitude becomes $O(\sigma^{10})$. The numerical results (discussed below) show that this term which also occurs in the analysis of Goldstein & Choi (1989), causes a rapid increase in the instability growth that ultimately ends in a singularity at a finite downstream position – indicating an explosive growth of the instability waves there. This explosive growth is then transferred to the plane wave through the back-reaction term and, to a greater degree, through the mutual interaction term in the plane-wave amplitude equation.

In summary then, the following picture begins to emerge from the analysis. Linear growth of the two-dimensional mode allows its amplitude to reach a level that produces a parametric resonance in the oblique modes which then allows them to grow at an accelerated rate until they become large enough to interact with themselves. This self-interaction (which was first analysed by Goldstein & Choi 1989)

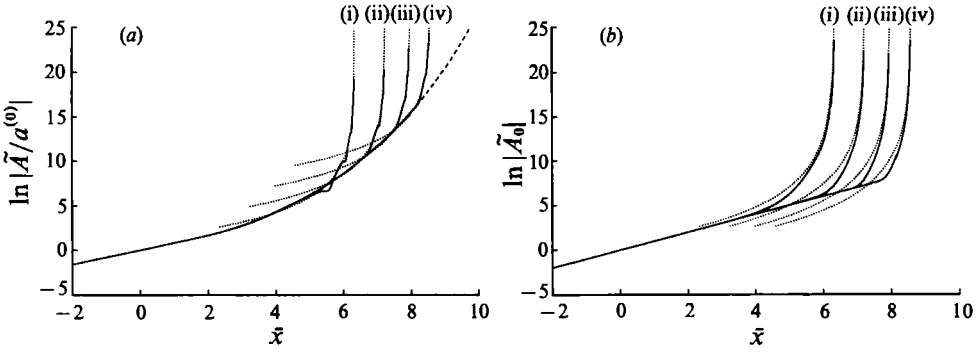

FIGURE 2. (*a*) $\ln|\tilde{A}/a^{(0)}|$ *vs.* $\bar{x}$, and (*b*) $\ln|\tilde{A}_0|$ *vs.* $\bar{x}$: $\arg(a^{(0)}) = 0$, $\tilde{\kappa}_i = 0$, and $|a^{(0)}| = 0.1, 0.01, 0.001, 0.0001$, curves (i)–(iv) respectively (——, numerical; · · · · · ·, local asymptotic; – – – –, parametric resonance).

produces a further enhancement in their growth, which ultimately ends in a singularity at a finite downstream position. This explosive growth is then transferred to the plane wave through the mutual interaction and back-reaction terms.

These conclusions are borne out by the numerical results shown in the following figures which are plots of the scaled instability wave amplitudes, $\tilde{A}$ and $\tilde{A}_0$, the instability wave growth rates, $|\tilde{A}|_{\bar{x}}/|\tilde{A}|$ and $|\tilde{A}_0|_{\bar{x}}/|\tilde{A}_0|$, and the scaled wavelength reductions, $\mathrm{Im}(\tilde{A}_{\bar{x}}/\tilde{A})$ and $\mathrm{Im}(\tilde{A}_{0\bar{x}}/\tilde{A}_0)$, as functions of the scaled streamwise coordinate $\bar{x}$.

The results were obtained by using the Adams–Moulton method (see Gear 1971, pp. 111–113) with variable (up to twelfth) order to advance the solutions downstream from the prescribed upstream linear states (5.56) and (5.57). The integral terms on the right-hand sides of (5.50) and (5.51) were computed by using the eleventh-order (9 point) Newton and Cotes' integration formula (see Kopal 1961, pp. 575–577) with the upstream 'tails' evaluated analytically from the upstream linear solutions.

Figure 2(*a*, *b*) illustrates the effect of varying the normalized initial amplitude ratio $|a^{(0)}|$. The initial wavenumber detuning and the argument of $a^{(0)}$ are set equal to zero. The results show that the scaled amplitudes initially exhibit linear growth and that the oblique-mode amplitudes begin to exhibit faster than exponential growth when the scaled streamwise coordinate $\bar{x}$ is equal to $\bar{x}_p \approx 0$, independently of $|a^{(0)}|$. This portion of the curve (as well as the linear portion) should be well described by the parametric resonance solution which is worked out in Appendix E and plotted as the dashed curve in figure 2(*a*). The plane wave, on the other hand, continues to exhibit linear growth until $\bar{x} = \bar{x}_n$, which is much larger than $\bar{x}_p$, with the exact value now depending on the choice of $|a^{(0)}|$.

The $|a^{(0)}|$ independence of $\bar{x}_p$ merely reflects the fact that the mutual interaction term makes a significant contribution to (5.50) when the plane-mode amplitude becomes large enough to satisfy (5.8) independently of the oblique-mode amplitudes (as long as their relative magnitudes are small enough to satisfy (7.1)). However, the $|a^{(0)}|$ dependence of $\bar{x}_n$ occurs because the fully interactive stage begins when the oblique-mode amplitude becomes large enough to satisfy (5.9) and the parametric resonance stage therefore becomes larger when $|a^{(0)}|$ becomes smaller, as shown in figure 2(*a*).

The scaled amplitudes of both the oblique mode and plane wave then exhibit a rapid increase in growth and ultimately end in a singularity at a point $\bar{x}_s$, whose exact location also depends on the choice of $|a^{(0)}|$ but is the same for both the oblique mode

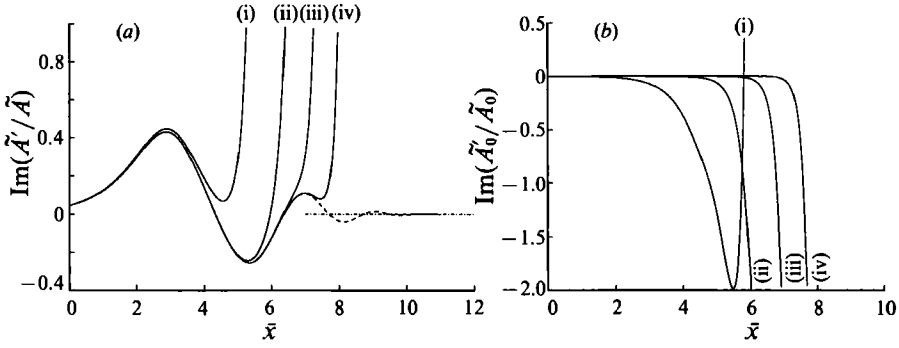

FIGURE 3. (*a*) $\mathrm{Im}\,(\tilde{A}'/\tilde{A})$ *vs.* $\bar{x}$, and (*b*) $\mathrm{Im}\,(\tilde{A}_0'/\tilde{A}_0)$ *vs.* $\bar{x}$: $\arg(a^{(0)}) = 0$, $\tilde{\kappa}_i = 0$, and $|a^{(0)}| = 0.1$, 0.01, 0.001, 0.0001, curves (i)–(iv) respectively (——, numerical; – – – –, parametric resonance; –·–·–, asymptotic parametric resonance).

and the plane wave. The flow is fully coupled in this region, in the sense that all of the nonlinear coupling terms now make a significant contribution to (5.50) and (5.51). The nonlinear increase in plane-wave amplitude is almost entirely due to the mutual interaction term in (5.51), which does not appear in the Craik (1971) and Smith & Stewart (1987) analyses and which is always much larger than the back-reaction term for the entire range of parameters considered herein. The plane-wave amplitudes increase monotonically in this nonlinear stage, but the oblique-mode amplitudes exhibit some oscillations. These oscillations, which also appeared in the weakly nonlinear results of Goldstein & Leib (1989) and Goldstein & Choi (1989) and the strongly nonlinear results of Goldstein & Hultgren (1988), are due to the nonlinear exchange of energy between modes that usually occurs within the critical layer. The dotted curves are obtained from the local asymptotic representations (6.1) and (6.2), which describe the solution in the vicinity of the singularity. The singularity location $\bar{x}_s$ is determined from the numerical solution. Notice that these curves, which do not exhibit any oscillation, still provide a fairly good representation for the oblique mode amplitudes over the entire range $\bar{x}_n < \bar{x} < \bar{x}_s$, but only provide a good representation for the plane-wave amplitudes when $\bar{x}$ is somewhat closer to $\bar{x}_s$. This is consistent with our observation that the singular nonlinear behaviour is initiated by the self-interaction term in the oblique-mode amplitude equation. It is also worth noting that the transition to fully coupled behaviour is very abrupt for the range of $|a^{(0)}|$ considered. The net effect of reducing $|a^{(0)}|$ is to delay both the onset of the fully coupled behaviour and the ultimate downstream location of the singularity.

The asymptotic solutions suggest that the present analysis will break down when $\bar{x}-\bar{x}_s$ is of the order of the wavelength scale X and that the flow in the inviscid wall layer (see §4) will then be fully nonlinear. It is easy to show that the next stage of evolution will then be governed by the inviscid, three-dimensional, unsteady triple-deck equations. The viscous flow near the wall will be governed by the three-dimensional unsteady boundary-layer equations and will probably separate.

Figure 3 (*a*, *b*) shows the scaled wavelength reduction versus the scaled streamwise coordinate for the same conditions used in figure 2. The parametric resonance solutions obtained from (E 6) and (E 7) are plotted as the dashed lines, and their asymptotic value, which is obtained from (7.2) is plotted as the dot-dashed curve. Notice that the numerical solutions always become fully interactive before the parametric resonance solutions reach their asymptotic stage.

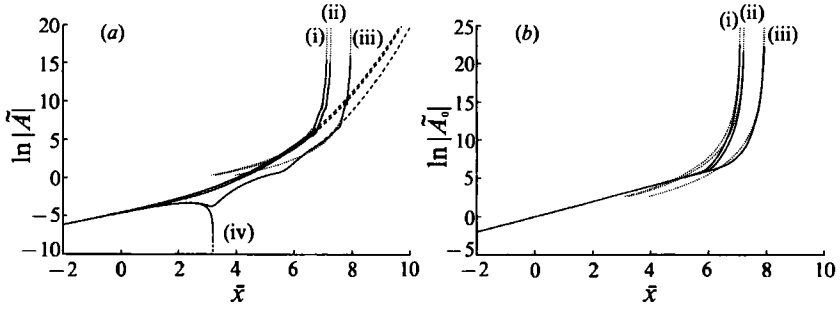

FIGURE 4. (*a*) $\ln|\tilde{A}|$ *vs.* $\bar{x}$, and (*b*) $\ln|\tilde{A}_0|$ *vs.* $\bar{x}$: $|a^{(0)}| = 0.01$, $\tilde{\kappa}_1 = 0$, and $\arg(a^{(0)}) = 45°$, 90°, 130°, 135°, curves (i)–(iv) respectively (——, numerical; · · · · · ·, local asymptotic; – – – –, parametric resonance).

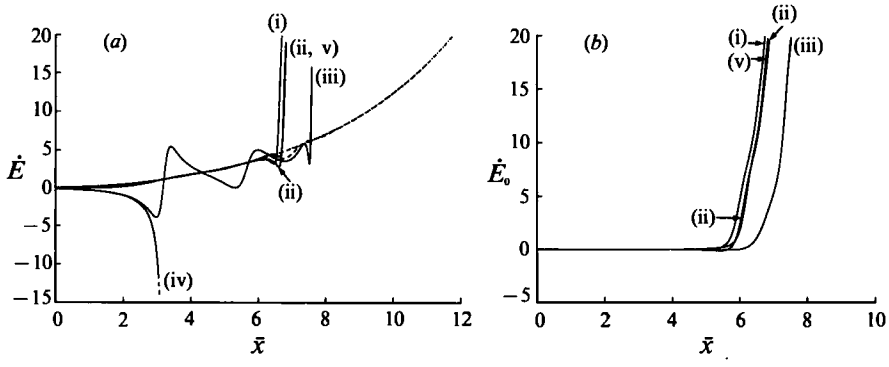

FIGURE 5. (*a*) $\dot{E}$ *vs.* $\bar{x}$, and (*b*) $\dot{E}_0$ *vs.* $\bar{x}$: $|a^{(0)}| = 0.01$, $\tilde{\kappa}_1 = 0$, and $\arg(a^{(0)}) = 45°$, 90°, 130°, 135°, 0°, curves (i)–(v) respectively (——, numerical; – – – –, parametric resonance; –·–·–, asymptotic parametric resonance).

Figure 4(*a*, *b*) shows the effect of varying $\arg(a^{(0)})$, the argument of $a^{(0)}$. Here we fix $|a^{(0)}| = 0.01$, typical of the values that might occur in the relevant experiments. The initial wavenumber detuning is still equal to zero. Notice that the $\arg(a^{(0)}) = 0$ results, which are shown in figure 2, are almost identical to the $\arg(a^{(0)}) = \frac{1}{2}\pi$ rad case. The net effect of varying $\arg(a^{(0)})$ between $\frac{1}{4}\pi$ and $\frac{3}{4}\pi$ rad is to delay the growth of the oblique-mode amplitude at the parametric resonance stage and, therefore, to move both the onset of the full interaction and the position of the singularity further downstream. These locations increase monotonically as $2\arg(a^{(0)})$ increases (or decreases) from $\frac{1}{2}\pi$ to $\frac{3}{2}\pi$ (or $-\frac{1}{2}\pi$) rad.

In order to explain the reduced growth and associated oscillations of the oblique-mode amplitudes that occur at the parametric resonance stage, it is useful to examine the nonlinear transfer rates of the instability wave energy, $\dot{E}$ and $\dot{E}_0$, which are twice the nonlinear growth rates,

$$\dot{E} \equiv (\mathrm{d}|\tilde{A}|^2/\mathrm{d}\bar{x})/|\tilde{A}|^2 - \tfrac{8}{5} = 2\,[\mathrm{Re}\,(\tilde{A}'/\tilde{A}) - \tfrac{4}{5}], \tag{7.3}$$

$$\dot{E}_0 \equiv (\mathrm{d}|\tilde{A}_0|^2/\mathrm{d}\bar{x})/|\tilde{A}_0|^2 - 2 = 2\,[\mathrm{Re}\,(\tilde{A}_0'/\tilde{A}_0) - 1]. \tag{7.4}$$

The oblique-mode amplitude equation (5.50) shows that $\dot{E}$ is determined by the mutual-interaction term during the parametric resonance stage since the self-interaction term is then much smaller than this term. Figure 5(*a*, *b*) shows $\dot{E}$ and $\dot{E}_0$ as functions of $\bar{x}$ for the conditions of figure 4. The figures also show (i) the analytical

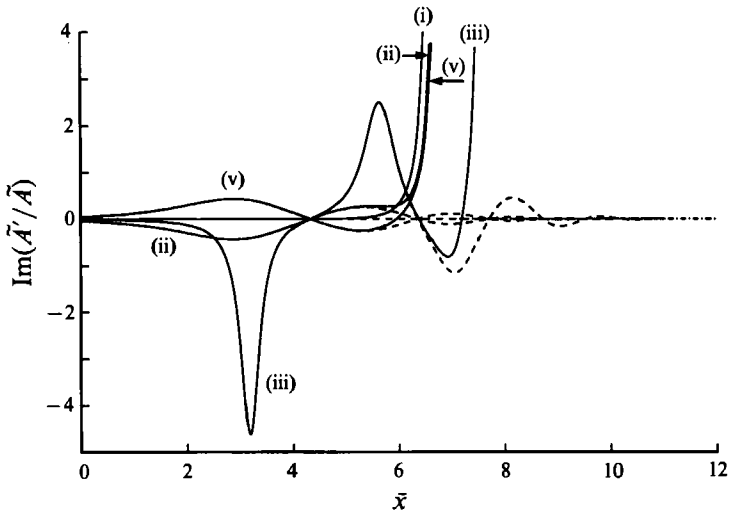

FIGURE 6. $\mathrm{Im}\,(\tilde{A}'/\tilde{A})$ *vs.* $\bar{x}$. $|a^{(0)}| = 0.01$, $\tilde{\kappa}_i = 0$, and $\arg(a^{(0)}) = 45°, 90°, 130°, 135°, 0°$, curves (i)–(v) respectively (——, numerical; – – –, parametric resonance; –·–·–, asymptotic parametric resonance).

parametric resonance solutions, which are obtained by substituting (E 6) and (E 7) into (7.3) and are plotted as the dashed curves and (ii) the asymptotic parametric resonance solution, which is obtained by substituting (7.2) into (7.3) and is plotted as the dot-dashed curve. The oblique modes gain energy throughout the entire parametric resonance region when $\arg(a^{(0)}) = \frac{1}{4}\pi$, $\frac{1}{2}\pi$, and 0 rad. However, the nonlinear mutual interaction causes the oblique modes to lose energy initially, but to gain it back later when $\arg(a^{(0)}) = \frac{13}{16}\pi$ rad. It is worth noting that parametric resonance solutions always approach the asymptotic solution (7.2) when $\arg(a^{(0)}) \neq \frac{3}{4}\pi$, while the full numerical solutions never reach this limit because (5.50) and (5.51) become fully interactive before this can occur.

A very dramatic change in behaviour occurs when $\arg(a^{(0)}) \approx \frac{3}{4}\pi$ rad, with the mutual interaction now causing the oblique modes to lose energy continuously and eventually causing a very rapid drop-off in their amplitudes at an $\bar{x}$ of about 3.19. Notice that this behaviour is well described by the analytical parametric resonance solution. However, the effect would probably be very hard to observe experimentally, since it occurs over a very small range of angles about $\frac{3}{4}\pi$. Nevertheless, it does provide an opportunity for artificially controlling instability-wave growth by manipulation of phase mismatch between modes.

Figure 6 shows the scaled wavelength reduction as function of the scaled streamwise coordinate for the same conditions used in figure 4(*a*). Computations based on both the analytical parametric resonance solution and the asymptotic parametric resonance solution are also shown in this figure. Notice that $\mathrm{Im}\,(\tilde{A}'/\tilde{A})$ for the $\arg(a^{(0)}) = 0$ case is almost identical to the negative of the $\arg(a^{(0)}) = \frac{1}{2}\pi$ result at the parametric resonance stage. The results again show that the fully coupled stage comes in well before the asymptotic exponential-of-an-exponential stage is reached.

Figures 7 and 8 illustrate the effect of initial wavenumber detuning away from the resonant condition $\bar{\beta}/\bar{\alpha} = \sqrt{3}/2$. The initial amplitude ratio $|a^{(0)}|$ is again set equal to 0.01, and the $\arg(a^{(0)})$ is set to zero. The results are similar to those discussed above

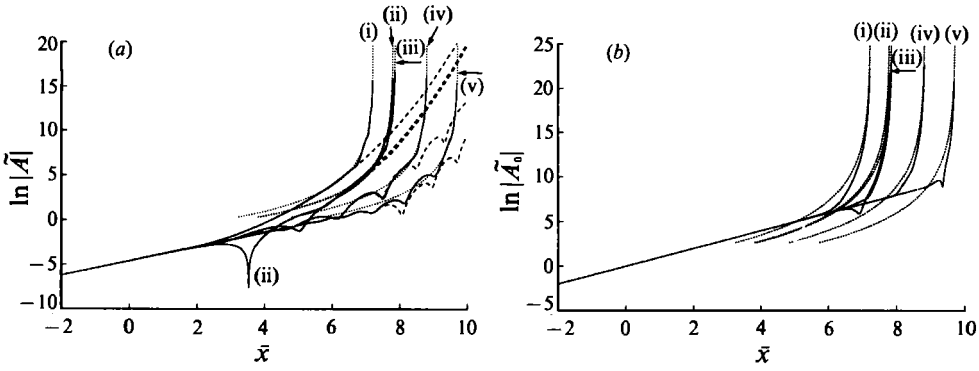

FIGURE 7. (*a*) $\ln|\tilde{A}|$ *vs.* $\bar{x}$, and (*b*) $\ln|\tilde{A}_0|$ *vs.* $\bar{x}$: $|a^{(0)}| = 0.01$, $\arg(a^{(0)}) = 0$, and $\tilde{\kappa}_1 = 0, 1, 2, 4, 8$, curves (i)–(v) respectively (——, numerical; ·····, local asymptotic; – – –, parametric resonance).

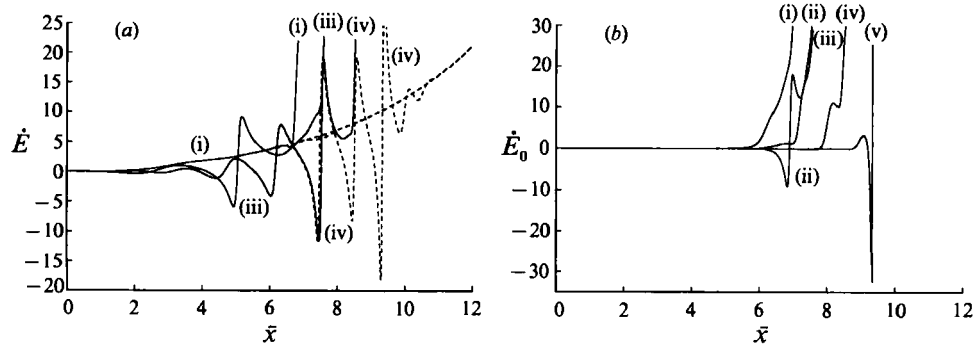

FIGURE 8. (*a*) $\dot{E}$ *vs.* $\bar{x}$, and (*b*) $\dot{E}_0$ *vs.* $\bar{x}$: $|a^{(0)}| = 0.01$, $\arg(a^{(0)}) = 0$, and $\tilde{\kappa}_1 = 0, 1, 2, 4, 8$, curves (i)–(v) respectively (——, numerical; – – –, parametric resonance).

in that increasing the initial wavenumber detuning now delays the growth in the oblique-mode amplitude and moves both the onset of the fully coupled stage and the singularity position further downstream. In fact, the oblique-mode amplitudes grow almost linearly, but with some oscillations, at the parametric resonance stage which appears when the detuning parameter $\tilde{\kappa}_1$ becomes greater than about 4. The oscillations at this stage are again due to the nonlinear exchange of energy between the oblique modes and plane wave, as can be seen from figure 8(*a*), which is a plot of $\dot{E}$ as defined in (7.3). Notice that the onset of full interaction becomes very abrupt at larger values of the detuning parameter. Figures 7(*a*) and 8(*a*) show that the parametric resonance solution becomes increasingly oscillatory as the initial wavenumber detuning is increased. The rapid drop-off in the oblique-mode amplitude, which occurred when $\arg(a^{(0)}) = \frac{3}{4}\pi$, is now observed when the detuning parameter $\tilde{\kappa}_1$ is equal to 1. However, in the present case, the wavenumber detuning eventually causes the oblique-mode amplitude ultimately to increase in magnitude.

The authors would like to thank Professor F. T. Smith for first suggesting and then strongly encouraging them to extend the analysis to the fully coupled case, Professor J. S. B. Gajjar for his helpful comments about extending the solution to low frequencies, and Drs Lennart S. Hultgren and David W. Wundrow for helping them with the extension to the case of a strongly nonlinear plane wave.

Appendix A

The detailed expressions for the terms on the right-hand sides of (5.16) and (5.17) are

$$G^{(2)} = 2\bar{\gamma}U_0' Y_c \cos Z(\mathrm{Re}\, \mathrm{i}A\, \mathrm{e}^{\mathrm{i}X/2})\, u^{(1)}_{\bar{\eta}\bar{\eta}} - (\bar{\alpha}u^{(1)}u^{(1)}_X + \bar{\beta}w^{(1)}u^{(1)}_Z)_{\bar{\eta}} + U_0'(\bar{\beta}w^{(2)}_Z - \bar{\eta}u^{(1)}_{\bar{\eta}x_1}), \tag{A 1}$$

$$H^{(2)} = 2\bar{\gamma}U_0' Y_c \cos Z(\mathrm{Re}\, \mathrm{i}A\, \mathrm{e}^{\mathrm{i}X/2})\, w^{(1)}_{\bar{\eta}} - (\bar{\alpha}u^{(1)}w^{(1)}_X + \bar{\beta}w^{(1)}w^{(1)}_Z) - U_0'\,\bar{\eta}w^{(1)}_{x_1} - \bar{\beta}p^{(2)}_Z, \tag{A 2}$$

$$G^{(3)} = 2\bar{\gamma}U_0' Y_c \cos Z(\mathrm{Re}\, \mathrm{i}A\, \mathrm{e}^{\mathrm{i}X/2})\, u^{(2)}_{\bar{\eta}\bar{\eta}} - [\bar{\alpha}(u^{(1)}u^{(2)})_X + u^{(1)}u^{(1)}_{x_1} + \bar{v}^{(2)}u^{(1)}_{\bar{\eta}} + \bar{\beta}(w^{(1)}u^{(2)}_Z + w^{(2)}u^{(1)}_Z)]_{\bar{\eta}} + U_0'(\bar{\beta}w^{(3)}_Z - \bar{\eta}u^{(2)}_{\bar{\eta}x_1}), \tag{A 3}$$

$$H^{(3)} = 2\bar{\gamma}U_0' Y_c \cos Z(\mathrm{Re}\, \mathrm{i}A\, \mathrm{e}^{\mathrm{i}X/2})\, w^{(2)}_{\bar{\eta}} - \bar{\alpha}(u^{(1)}w^{(2)}_X + u^{(2)}w^{(1)}_X) - u^{(1)}w^{(1)}_{x_1} - \bar{v}^{(2)}w^{(1)}_{\bar{\eta}} - \bar{\beta}[(w^{(1)}w^{(2)})_Z + p^{(3)}_Z] - U_0'\,\bar{\eta}w^{(2)}_{x_1}, \tag{A 4}$$

$$G^{(4)} = 2\bar{\gamma}U_0' Y_c \cos Z(\mathrm{Re}\, \mathrm{i}A\, \mathrm{e}^{\mathrm{i}X/2})\, u^{(3)}_{\bar{\eta}\bar{\eta}} - [\bar{\alpha}(u^{(1)}u^{(3)} + \tfrac{1}{2}u^{(2)}u^{(2)})_X + (u^{(1)}u^{(2)})_{x_1} + \bar{v}^{(2)}u^{(2)}_{\bar{\eta}} + \bar{v}^{(3)}u^{(1)}_{\bar{\eta}} + \bar{\beta}(w^{(1)}u^{(3)}_Z + w^{(2)}u^{(2)}_Z + w^{(3)}u^{(1)}_Z)]_{\bar{\eta}} + U_0'(\bar{\beta}w^{(4)}_Z - \bar{\eta}u^{(3)}_{\bar{\eta}x_1}). \tag{A 5}$$

Appendix B

The expressions for the terms on the right-hand sides of (5.37)–(5.39) are

$$\mathscr{G}^{(2)}_{0,0} = (Y_c/\bar{c}^2)(\tan\theta \sec\theta) A Q^{(1)*}_{\eta\eta}, \tag{B 1}$$

$$\mathscr{H}^{(2)}_{0,0} = 0, \tag{B 2}$$

$$\mathscr{G}^{(2)}_{0,2} = 2\mathrm{i}\tan\theta[W^{(2)}_{0,2} - (\mathrm{i}Y_c/2\bar{c}^2)(\sec\theta)\,\mathrm{Re}\,(AQ^{(1)*}_{\eta\eta})], \tag{B 3}$$

$$\mathscr{H}^{(2)}_{0,2} = (\mathrm{i}Y_c/\bar{c}^2)\sec\theta[(2\bar{c}/U_0'Y_c)(\sin\theta)|Q^{(1)}|^2 + \mathrm{Im}\,(AQ^{(1)*}_{\eta})], \tag{B 4}$$

$$\mathscr{G}^{(2)}_{1,1} = -(\tan\theta)\,\mathrm{L}_1(W^{(2)}_{1,1} + U_0'Q^{(1)}_{\tilde{x}})_{\eta}, \tag{B 5}$$

$$\mathscr{H}^{(2)}_{1,1} = -\frac{\mathrm{i}}{U_0'\bar{c}}(\tan\theta)P^{(2)}_{1,1} - U_0'\left(\frac{\partial}{\partial\tilde{x}} + \frac{\mathrm{i}\bar{\mu}^{\dagger}_c Y_c}{U_0'^2}\right)\mathrm{L}_1\left(\eta Q^{(1)}_{\eta} + \frac{2\mathrm{i}\bar{\lambda}}{3}Q^{(1)}_{\eta\eta\eta}\right), \tag{B 6}$$

$$\mathscr{G}^{(2)}_{2,0} = (Y_c/\bar{c}^2)\tan\theta\sec\theta[(2\mathrm{i}\bar{c}/U_0'Y_c)(\sin\theta)Q^{(1)^2} - AQ^{(1)}_{\eta}]_{\eta}, \tag{B 7}$$

$$\mathscr{H}^{(2)}_{2,0} = 0, \tag{B 8}$$

$$\mathscr{G}^{(2)}_{2,2} = -(\tan\theta)\,\mathrm{L}_2 W^{(2)}_{2,2\eta}, \tag{B 9}$$

$$\mathscr{H}^{(2)}_{2,2} = (Y_c/2\bar{c}^2)(\sec\theta)AQ^{(1)}_{\eta}, \tag{B 10}$$

$$\mathscr{R}^{(3)}_{1,1} = \mathrm{i}Y_c\sec\theta\{(\bar{\mu} - \tfrac{1}{4}\bar{c}^2)A + (1/2\bar{c}^2)[A(2\,\mathrm{Re}\,Q^{(2)}_{0,0} + Q^{(2)}_{0,2} + \tan\theta\, W^{(2)}_{0,2\eta}) - A^*Q^{(2)}_{2,0}]_{\eta}\} + \frac{2}{\bar{c}U_0'}\tan\theta[Q^{(1)}U^{(2)}_{0,2} - \frac{\mathrm{i}}{\bar{\alpha}\bar{c}}(Q^{(1)}_{\eta}V^{(2)}_{0,2} - Q^{(1)*}_{\eta}V^{(2)}_{2,0})]_{\eta}, \tag{B 11}$$

$$\mathscr{H}^{(3)}_{1,1} = -(1/2U_0'\bar{c})\{Q^{(1)}(2\,\mathrm{Re}\,U^{(2)}_{0,0} - U^{(2)}_{0,2} - \tan\theta\, W^{(2)}_{0,2}) - Q^{(1)*}U^{(2)}_{2,0} + 2\mathrm{i}/\bar{\alpha}\bar{c} \times [Q^{(1)}_{\eta}V^{(2)}_{0,2} - Q^{(1)*}_{\eta}V^{(2)}_{2,0} - U_0'Y_c\bar{\gamma}(AW^{(2)}_{0,2} - A^*W^{(2)}_{2,2})_{\eta}]\} + \ldots, \tag{B 12}$$

$$\mathscr{G}^{(3)}_{3,1} = -\tfrac{1}{3}\tan\theta\left\{\mathrm{L}_3 W^{(3)}_{3,1\eta} - \frac{4}{U_0'\bar{c}}\left[Q^{(1)}(U^{(2)}_{2,0} + 2U^{(2)}_{2,2}) - \frac{\mathrm{i}}{2\bar{\alpha}\bar{c}}Q^{(1)}_{\eta}V^{(2)}_{2,0} + \frac{3\mathrm{i}U_0'Y_c}{8\bar{c}\sin\theta}A(Q^{(2)}_{2,0} - \tfrac{2}{3}\tan\theta\, W^{(2)}_{2,2\eta})\right]_{\eta}\right\}, \tag{B 13}$$

$$\mathscr{H}^{(3)}_{3,1} = -(1/2U_0'\bar{c})[Q^{(1)}(U^{(2)}_{2,0} - 2\tan\theta\, W^{(2)}_{2,2}) - (2\mathrm{i}/\bar{\alpha}\bar{c})(Q^{(1)}_{\eta}V^{(2)}_{2,0} + U_0'Y_c\bar{\gamma}AW^{(2)}_{2,2\eta})], \tag{B 14}$$

$$\begin{aligned}\mathscr{G}^{(4)}_{2,0} = &-(2/U_0'\bar{\alpha})(\bar{\mu}-\tfrac{1}{4}\bar{c}^2)\,V^{(2)}_{2,0}-(2\mathrm{i}/U_0'\bar{c})\{U^{(2)}_{2,0}\,\mathrm{Re}\,U^{(2)}_{0,0}+U^{(2)}_{2,2}(U^{(2)}_{0,2}-\tan\theta\,W^{(2)}_{0,2})\\ &+\tfrac{1}{2}U^{(2)}_{1,1}(U^{(2)}_{1,1}-\tan\theta\,W^{(3)}_{1,1})-\tan\theta\,U^{(2)}_{0,2}\,W^{(2)}_{2,2}-(\mathrm{i}/\bar{\alpha}\bar{c})\,(Q^{(2)}_{2,2}\,V^{(2)}_{0,2}+Q^{(2)}_{1,1}\,V^{(2)}_{1,1}\\ &+V^{(2)}_{2,0}\,\mathrm{Re}\,Q^{(2)}_{0,0})+\tfrac{1}{2}\mathrm{i}\tan\theta[Q^{(1)}(3U^{(3)}_{1,1}-\tan\theta\,W^{(3)}_{1,1})\\ &-Q^{(1)*}(U^{(3)}_{3,1}-\tan\theta\,W^{(3)}_{3,1})-(2\mathrm{i}/\bar{\alpha}\bar{c})\,(Q^{(1)}_{\eta}\,V^{(3)}_{1,1}-Q^{(1)*}_{\eta}\,V^{(3)}_{3,1})\\ &+(\mathrm{i}U_0'\,Y_c/\bar{c}\sin\theta)\,(AQ^{(3)}_{1,1}-A^{*}Q^{(3)}_{3,1})]\}_{\eta}+\ldots, \qquad \text{(B 15)}\end{aligned}$$

where

$$U^{(l)}_{n,m\eta} = Q^{(l)}_{n,m}, \qquad \text{(B 16)}$$

$$V^{(2)}_{0,2\eta} = -2\mathrm{i}\bar{\beta}\bar{c}W^{(2)}_{0,2}, \qquad \text{(B 17)}$$

$$V^{(2)}_{1,1\eta} = -\mathrm{i}U_0'\,\bar{\gamma}\bar{c}A, \qquad \text{(B 18)}$$

$$V^{(2)}_{2,0\eta} = -\mathrm{i}\bar{\alpha}\bar{c}U^{(2)}_{2,0}, \qquad \text{(B 19)}$$

$$V^{(3)}_{1,1\eta} = -\tfrac{1}{2}\mathrm{i}\bar{\alpha}\bar{c}(U^{(3)}_{1,1}+\tan\theta\,W^{(3)}_{1,1}-\mathrm{i}U_0'\,U^{(2)}_{1,1_{\tilde{x}}}), \qquad \text{(B 20)}$$

$$V^{(3)}_{3,1\eta} = -\tfrac{3}{2}\mathrm{i}\bar{\alpha}\bar{c}(U^{(3)}_{3,1}+\tfrac{1}{3}\tan\theta\,W^{(3)}_{3,1}), \qquad \text{(B 21)}$$

$$P^{(2)}_{1,1\eta} = 0, \qquad \text{(B 22)}$$

and the asterisks denote the complex conjugates. We have used the fact that

$$Q^{(l)}_{n,m} = Q^{(l)}_{n,-m}, \quad W^{(l)}_{n,m} = -W^{(l)}_{n,-m} \quad \text{for} \quad l = 2,3 \text{ and } n \neq 0, \qquad \text{(B 23)}$$

$$Q^{(2)}_{0,2} = Q^{(2)*}_{0,2}, \quad W^{(2)}_{0,2} = -W^{(2)*}_{0,2}, \qquad \text{(B 24)}$$

and anticipated the fact that the relevant solutions to (5.37) and (5.38) along with (B 2), (B 5), (B 8), and (B 9) are the trivial solutions

$$W^{(2)}_{0,0} = W^{(2)}_{2,0} = 0, \qquad \text{(B 25)}$$

$$Q^{(2)}_{1,1} = -\tan\theta(W^{(2)}_{1,1}+U_0'\,Q^{(1)}_{\tilde{x}})_{\eta}, \qquad \text{(B 26)}$$

$$Q^{(2)}_{2,2} = -\tan\theta\,W^{(2)}_{2,2\eta}. \qquad \text{(B 27)}$$

The dots in (B 12) and (B 15) represent the terms which do not play any active role in calculating the velocity jump of the two-dimensional wave across the critical layer.

Appendix C

In this appendix we determine $Q^{(1)}$, $Q^{(l)}_{n,m}$, $W^{(l)}_{n,m}$, $q^{(3)}_{1,1}$, $\int_{-\infty}^{\infty} q^{(3)}_{1,1}\,\mathrm{d}\eta$, and $\int_{-\infty}^{\infty} Q^{(4)}_{2,0}\,\mathrm{d}\eta$ for the inviscid case.

It follows from (5.27) to (5.29) that

$$Q^{(1)} = \sin\theta\,\mathrm{e}^{-\mathrm{i}\eta\tilde{x}}\,I_0(\eta,\tilde{x}), \qquad \text{(C 1)}$$

where we have put

$$I_n(\eta,\tilde{x}) \equiv \int_{-\infty}^{\tilde{x}} \mathrm{e}^{\mathrm{i}\eta\tilde{x}_1}(\tilde{x}-\tilde{x}_1)^n\,A(\tilde{x}_1)\,\mathrm{d}\tilde{x}_1 \quad \text{for} \quad n = 0,1,2,\ldots. \qquad \text{(C 2)}$$

It is worth noticing that

$$Q^{(1)} \to \frac{-\mathrm{i}\sin\theta}{\eta-\mathrm{i}\kappa}\,\mathrm{e}^{\kappa\tilde{x}}$$

when

$$A \to \mathrm{e}^{\kappa\tilde{x}}$$

so that (5.25) and (5.26) approach the linear critical-layer solution when A approaches the linear upstream condition.

Inserting (C 1) along with (B 22) into (B 1), (B 4), (B 6), (B 7), and (B 10) and integrating (5.37) and (5.38), we obtain

$$Q^{(2)}_{0,0} = -(Y_c/\bar{c}^2)\tan^2\theta J_{02}(\eta,\tilde{x}), \tag{C 3}$$

$$W^{(2)}_{0,2} = (\mathrm{i}Y_c/\bar{c}^2)\tan\theta\,\mathrm{Re}\,[J_{01}(\eta,\tilde{x})+4\Lambda J_{10}(\eta,\tilde{x})], \tag{C 4}$$

$$W^{(2)}_{1,1} = -\mathrm{i}U_0'\sin\theta\left\{\frac{\sec\theta}{U_0'^2\,\bar{c}}\mathrm{e}^{-\mathrm{i}\eta\tilde{x}}\int_{-\infty}^{\tilde{x}}\mathrm{e}^{\mathrm{i}\eta\tilde{x}_1}P^{(2)}_{1,1}(\tilde{x}_1)\,\mathrm{d}\tilde{x}_1 - \eta\left(\frac{\partial}{\partial\tilde{x}}+\frac{\mathrm{i}\bar{\mu}^{\dagger}_c Y_c}{U_0'^2}\right)[\mathrm{e}^{-\mathrm{i}\eta\tilde{x}}I_1(\eta,\tilde{x})]\right\}, \tag{C 5}$$

$$Q^{(2)}_{2,0} = (Y_c/\bar{c}^2)(\tan^2\theta)\,\mathrm{e}^{-2\mathrm{i}\eta\tilde{x}}[I_0(\eta,\tilde{x})I_2(\eta,\tilde{x})-(1-2\Lambda)I_1^2(\eta,\tilde{x})], \tag{C 6}$$

$$W^{(2)}_{2,2} = -(\mathrm{i}Y_c/2\bar{c}^2)(\tan\theta)\,\mathrm{e}^{-2\mathrm{i}\eta\tilde{x}}K_{01}(\eta,\tilde{x}), \tag{C 7}$$

where we have put

$$\Lambda \equiv (\bar{c}/U_0'\,Y_c)\sin^2\theta, \tag{C 8}$$

$$J_{mn}(\eta,\tilde{x}) \equiv \int_{-\infty}^{\tilde{x}}\mathrm{e}^{\mathrm{i}\eta\tilde{x}_1}(\tilde{x}-\tilde{x}_1)^m A(\tilde{x}_1)I_n^*(\eta,\tilde{x}_1)\,\mathrm{d}\tilde{x}_1 \quad \text{for} \quad m,n=0,1,2,\ldots, \tag{C 9}$$

$$K_{mn}(\eta,\tilde{x}) \equiv \int_{-\infty}^{\tilde{x}}\mathrm{e}^{\mathrm{i}\eta\tilde{x}_1}(\tilde{x}-\tilde{x}_1)^m A(\tilde{x}_1)I_n(\eta,\tilde{x}_1)\,\mathrm{d}\tilde{x}_1 \quad \text{for} \quad m,n=0,1,2,\ldots, \tag{C 10}$$

and the asterisk denotes the complex conjugate. Inserting (C 1) and (C 4) into (B 3) and integrating (5.37) yields

$$Q^{(2)}_{0,2} = -(Y_c/\bar{c}^2)\tan^2\theta\,\mathrm{Re}\,[J_{02}(\eta,\tilde{x})+2J_{11}(\eta,\tilde{x})+4\Lambda J_{20}(\eta,\tilde{x})]. \tag{C 11}$$

Substituting (C 4) and (C 6) along with (B 16) into (B 17) and (B 19) we find that

$$V^{(2)}_{0,2} = r^{(2)}_{0,2\tilde{x}}(\eta,\tilde{x}), \tag{C 12}$$

and

$$V^{(2)}_{2,0} = -\mathrm{i}\bar{\alpha}U_0'\,Y_c A_0(\tilde{x}) - \tfrac{1}{2}\bar{\alpha}\bar{c}\,\mathrm{e}^{-2\mathrm{i}\eta\tilde{x}}\{[\mathrm{e}^{2\mathrm{i}\eta\tilde{x}}U^{(2)}_{2,0}(\eta,\tilde{x})]_{\tilde{x}} - (\mathrm{i}Y_c/\bar{c}^2)\tan^2\theta[\mathrm{e}^{\mathrm{i}\eta\tilde{x}}A(\tilde{x})I_1(\eta,\tilde{x})+2\Lambda I_0^2(\eta,\tilde{x})]\}, \tag{C 13}$$

where

$$r^{(2)}_{0,2\eta} = (\bar{\alpha}Y_c/\bar{c})\tan^2\theta\,\mathrm{Re}\,[J_{11}(\eta,\tilde{x})+2\Lambda J_{20}(\eta,\tilde{x})]. \tag{C 14}$$

Inserting (C 1), (C 3), (C 4), (C 6), and (C 11)–(C 13) into (B 11) and integrating (5.39), we obtain

$$\begin{aligned} q^{(3)}_{1,1} = -\frac{Y_c}{\bar{c}^2}(\sec\theta)\,\mathrm{e}^{-\mathrm{i}\eta\tilde{x}}\Bigg[&2\sin^2\theta\int_{-\infty}^{\tilde{x}}\mathrm{e}^{2\mathrm{i}\eta\tilde{x}_1}A_0(\tilde{x}_1)I_2^*(\eta,\tilde{x}_1)\,\mathrm{d}\tilde{x}_1 \\ &-\mathrm{i}\left(\bar{\mu}-\frac{\bar{c}^2}{4}\right)\bar{c}^2 I_0(\eta,\tilde{x})-\mathrm{i}\Lambda[I_2^*(\eta,\tilde{x})\,\mathrm{e}^{2\mathrm{i}\eta\tilde{x}}U^{(2)}_{2,0}(\eta,\tilde{x})+\frac{2}{\bar{\alpha}\bar{c}}I_2(\eta,\tilde{x})\,r^{(2)}_{0,2}(\eta,\tilde{x})] \\ &+\frac{Y_c}{2\bar{c}^2}\tan^2\theta\Bigg\{[I_1(\eta,\tilde{x})f_1(\eta,\tilde{x})]_{\tilde{x}}+\Lambda[I_0(\eta,\tilde{x})f_2(\eta,\tilde{x}) \\ &-8\mathrm{i}I_1(\eta,\tilde{x})\,\mathrm{Im}\,J_{11}(\eta,\tilde{x})]-\int_{-\infty}^{\tilde{x}}\mathrm{e}^{\mathrm{i}\eta\tilde{x}_1}A(\tilde{x}_1)f_3(\eta,\tilde{x}_1)\,\mathrm{d}\tilde{x}_1 \\ &+\int_{-\infty}^{\tilde{x}}\mathrm{e}^{-\mathrm{i}\eta\tilde{x}_1}A^*(\tilde{x}_1)[I_0(\eta,\tilde{x}_1)I_3(\eta,\tilde{x}_1)-(1-4\Lambda)I_1(\eta,\tilde{x}_1)I_2(\eta,\tilde{x}_1)]\,\mathrm{d}\tilde{x}_1\Bigg\}\Bigg], \end{aligned} \tag{C 15}$$

where
$$f_1(\eta,\tilde{x}) = 2\Lambda[J_{21}(\eta,\tilde{x})+\tfrac{4}{3}\Lambda\,\mathrm{Re}\,J_{30}(\eta,\tilde{x})], \tag{C 16}$$

$$f_2(\eta,\tilde{x}) = 4[\mathrm{Re}\,J_{12}(\eta,\tilde{x})-\tfrac{1}{3}\Lambda I_0(\eta,\tilde{x})\,I_3^*(\eta,\tilde{x})], \tag{C 17}$$

$$f_3(\eta,\tilde{x}) = f_1(\eta,\tilde{x})+J_{03}(\eta,\tilde{x})+2\Lambda[I_1(\eta,\tilde{x})\,I_2^*(\eta,\tilde{x})+f_2(\eta,\tilde{x})] + 2\mathrm{i}\,\mathrm{Im}\,[J_{03}(\eta,\tilde{x})+J_{12}(\eta,\tilde{x})+2\Lambda J_{21}(\eta,\tilde{x})]. \tag{C 18}$$

Integrating (C 15) and substituting the result into (5.41), we can obtain the amplitude equation for A.

Inserting (C 1)–(C 4), (C 6), (C 7), and (C 11)–(C 13) into (B 12) and integrating (5.38) yields

$$\begin{aligned} W_{1,1}^{(3)} = {} & \frac{\mathrm{i}Y_c}{2\bar{c}^2}(\sin\theta)\,\mathrm{e}^{-\mathrm{i}\eta\tilde{x}}\Bigg[2\int_{-\infty}^{\tilde{x}}\mathrm{e}^{2\mathrm{i}\eta\tilde{x}_1}A_0(\tilde{x}_1)\,I_1^*(\eta,\tilde{x}_1)\,\mathrm{d}\tilde{x}_1 \\ & -\frac{\mathrm{i}\bar{c}}{U_0'\,Y_c}[I_1^*(\eta,\tilde{x})\,\mathrm{e}^{2\mathrm{i}\eta\tilde{x}}\,U_{2,0}^{(2)}(\eta,\tilde{x})-\frac{2}{\bar{\alpha}\bar{c}}I_1(\eta,\tilde{x})\,r_{0,2}^{(2)}(\eta,\tilde{x})]+\frac{Y_c}{\bar{c}^2}\sec^2\theta \\ & \times\Bigg\{I_0(\eta,\tilde{x})\,[\tfrac{1}{4}f_{1\tilde{x}}(\eta,\tilde{x})-2\mathrm{i}\Lambda\,\mathrm{Im}\,J_{11}(\eta,\tilde{x})-\Lambda^2 I_0(\eta,\tilde{x})\,I_2^*(\eta,\tilde{x})] \\ & -\int_{-\infty}^{\tilde{x}}\mathrm{e}^{\mathrm{i}\eta\tilde{x}_1}A(\tilde{x}_1)f_4(\eta,\tilde{x}_1)\,\mathrm{d}\tilde{x}_1+\int_{-\infty}^{\tilde{x}}\mathrm{e}^{-\mathrm{i}\eta\tilde{x}_1}A^*(\tilde{x}_1)\,[\tfrac{1}{2}K_{02}(\eta,\tilde{x}_1) \\ & +K_{11}(\eta,\tilde{x}_1)]\,\mathrm{d}\tilde{x}_1\Bigg\}\Bigg]+\ldots, \end{aligned} \tag{C 19}$$

where

$$f_4(\eta,\tilde{x}) = \tfrac{1}{4}f_{1\tilde{x}}(\eta,\tilde{x})+\Lambda[|I_1(\eta,\tilde{x})|^2-2\Lambda I_0(\eta,\tilde{x})\,I_2^*(\eta,\tilde{x})] + \mathrm{i}\,\mathrm{Im}\,[J_{02}(\eta,\tilde{x})+2\Lambda J_{11}(\eta,\tilde{x})], \tag{C 20}$$

and the dots in (C 19) represent the terms which do not play any active role in calculating the plane-wave velocity jump across the critical layer. Substituting (5.40), (B 26), (C 5), and (C 15) into (B 20) we find

$$\begin{aligned} V_{1,1}^{(3)} = {} & -\tfrac{1}{2}\bar{\alpha}\bar{c}\,\mathrm{e}^{-\mathrm{i}\eta\tilde{x}}[\mathrm{e}^{\mathrm{i}\eta\tilde{x}}\,r_{1,1}^{(3)}(\eta,\tilde{x})]_{\tilde{x}}-(Y_c/\bar{c}^2)\,\Lambda(\sec\theta)\,\mathrm{e}^{-\mathrm{i}\eta\tilde{x}}\Bigg[2I_0(\eta,\tilde{x})\,r_{0,2}^{(2)}(\eta,\tilde{x}) \\ & +I_1(\eta,\tilde{x})\,r_{0,2\tilde{x}}^{(2)}(\eta,\tilde{x})+I_1^*(\eta,\tilde{x})\,\mathrm{e}^{2\mathrm{i}\eta\tilde{x}}\,V_{2,0}^{(2)}(\eta,\tilde{x})+\frac{\mathrm{i}\bar{\alpha}U_0'\,Y_c^2}{4\bar{c}^2}\sec^2\theta \\ & \times\{\mathrm{e}^{\mathrm{i}\eta\tilde{x}}A(\tilde{x})f_5(\eta,\tilde{x})+\mathrm{e}^{-\mathrm{i}\eta\tilde{x}}A^*(\tilde{x})\,[I_0(\eta,\tilde{x})\,I_2(\eta,\tilde{x}) \\ & -(1-2\Lambda)\,I_1^2(\eta,\tilde{x})]-4\mathrm{i}\Lambda I_0(\eta,\tilde{x})\,\mathrm{Im}\,J_{01}(\eta,\tilde{x})\}\Bigg]+\ldots, \end{aligned} \tag{C 21}$$

where
$$r_{1,1\eta}^{(3)} = q_{1,1}^{(3)}, \tag{C 22}$$

$$f_5(\eta,\tilde{x}) = 2J_{02}(\eta,\tilde{x})+J_{02}^*(\eta,\tilde{x})-2\mathrm{i}(1-2\Lambda)\,\mathrm{Im}\,J_{11}(\eta,\tilde{x})+(1/2\Lambda)f_{1\tilde{x}}(\eta,\tilde{x}), \tag{C 23}$$

and we have omitted the terms which do not play any active role in calculating the fundamental mode velocity jump.

Inserting (B 27), (C 1), (C 6), (C 7), and (C 13) into (B 13) and (B 14) and integrating (5.37), (5.38), and (B 21), we obtain

$$Q^{(3)}_{3,1} = -\tfrac{1}{3}\tan\theta W^{(3)}_{3,1\eta} + \frac{Y_c}{3\bar{c}^2}(\sec\theta)\,e^{-3i\eta\tilde{x}}\Big[2\sin^2\int_{-\infty}^{\tilde{x}} e^{2i\eta\tilde{x}_1}A_0(\tilde{x}_1)\,I_2(\eta,\tilde{x}_1)\,d\tilde{x}_1$$
$$-i\Lambda I_2(\eta,\tilde{x})\,e^{2i\eta\tilde{x}}\,U^{(2)}_{2,0}(\eta,\tilde{x}) + (2Y_c/\bar{c}^2)\,\Lambda\tan^2\theta\Big\{I_1(\eta,\tilde{x})\,[4K_{11}(\eta,\tilde{x})$$
$$+(4-\Lambda)K_{02}(\eta,\tilde{x}) + \Lambda I_1^2(\eta,\tilde{x})] - I_2(\eta,\tilde{x})\,K_{01}(\eta,\tilde{x})$$
$$+\frac{1}{2\Lambda}\int_{-\infty}^{\tilde{x}} e^{i\eta\tilde{x}_1}A(\tilde{x}_1)\,[K_{12}(\eta,\tilde{x}_1) + 2K_{21}(\eta,\tilde{x}_1) + 2I_0(\eta,\tilde{x}_1)\,I_3(\eta,\tilde{x}_1)$$
$$-(2+\Lambda-2\Lambda^2)\,I_1(\eta,\tilde{x}_1)\,I_2(\eta,\tilde{x}_1)]\,d\tilde{x}_1\Big\}\Big], \tag{C 24}$$

$$W^{(3)}_{3,1} = -\frac{iY_c}{\bar{c}^2}(\sin\theta)\,e^{-3i\eta\tilde{x}}\Big[\int_{-\infty}^{\tilde{x}} e^{2i\eta\tilde{x}_1}A_0(\tilde{x}_1)\,I_1(\eta,\tilde{x}_1)\,d\tilde{x}_1$$
$$-\frac{i\bar{c}}{2U_0'\,Y_c}I_1(\eta,\tilde{x})\,e^{2i\eta\tilde{x}}\,U^{(2)}_{2,0}(\eta,\tilde{x}) + \frac{Y_c}{4\bar{c}^2}\sec^2\theta\Big\{\Lambda I_0(\eta,\tilde{x})f_6(\eta,\tilde{x})$$
$$+\int_{-\infty}^{\tilde{x}} e^{i\eta\tilde{x}_1}A(\tilde{x}_1)\,[K_{02}(\eta,\tilde{x}_1) + (1-\Lambda)f_6(\eta,\tilde{x}_1)]\,d\tilde{x}_1\Big\}\Big], \tag{C 25}$$

$$V^{(3)}_{3,1} = -\tfrac{1}{2}\bar{\alpha}\bar{c}\,e^{-3i\eta\tilde{x}}\{e^{3i\eta\tilde{x}}\,[U^{(3)}_{3,1}(\eta,\tilde{x}) + \tfrac{1}{3}\tan\theta W^{(3)}_{3,1}(\eta,\tilde{x})]\}_{\tilde{x}} + (\bar{\alpha}Y_c/3\bar{c})\,\Lambda(\sec\theta)$$
$$\times e^{-3i\eta\tilde{x}}\,[e^{2i\eta\tilde{x}}\,[2I_0(\eta,\tilde{x})\,U^{(2)}_{2,0}(\eta,\tilde{x}) - \frac{1}{\bar{\alpha}\bar{c}}I_1(\eta,\tilde{x})\,V^{(2)}_{2,0}(\eta,\tilde{x})] + (iU_0'\,Y_c^2/2\bar{c}^3)\sec^2\theta$$
$$\times\{e^{i\eta\tilde{x}}A(\tilde{x})\,[2K_{02}(\eta,\tilde{x}) + K_{11}(\eta,\tilde{x}) + 3\Lambda I_1^2(\eta,\tilde{x})] + 4\Lambda I_0(\eta,\tilde{x})\,K_{01}(\eta,\tilde{x})\}], \tag{C 26}$$

where
$$f_6(\eta,\tilde{x}) = 2[K_{11}(\eta,\tilde{x}) - \Lambda I_1^2(\eta,\tilde{x})]. \tag{C 27}$$

Inserting (B 18), (B 26), (B 27), (C 1), (C 3)–(C 7), (C 11)–(C 13), (C 15), (C 19), (C 21) and (C 24) to (C 26) along with (B 16) into (B 15) and integrating (5.37), we can obtain $Q^{(4)}_{2,0}$ after some manipulation. Integrating $Q^{(4)}_{2,0}$ and substituting the result into (5.42), we obtain the amplitude equation for A_0.

Appendix D

The detailed expressions for D_n in (6.3)–(6.6) are

$$D_1 = \frac{2}{5}\int_1^\infty \frac{(u-1)^2}{u^{4+2i\psi}(2u-1)^{3-i\psi}}\,du, \tag{D 1}$$

$$D_2 = \frac{1}{10}\int_1^\infty\int_u^\infty \frac{(u-1)\,[2(u-1)^2 - (u-1)\,(v-1) + 3(v-1)^2]}{u^{3+i\psi}v^{3+i\psi}(u+v-1)^{3-i\psi}}\,dv\,du, \tag{D 2}$$

$$D_3 = \int_1^\infty\int_u^\infty (u-1)\Big[\frac{2(u-1)^2}{u^{4+2i\psi}v^{3+i\psi}(2u+v-2)^{3-i\psi}} + \frac{(u+v-2)\,(v-1)}{u^{3+i\psi}v^{4+2i\psi}(u+2v-2)^{3-i\psi}}\Big]\,dv\,du, \tag{D 3}$$

$$D_4 = \frac{1}{4}\int_1^\infty\int_u^\infty\int_v^\infty \frac{1}{u^{3+i\psi}v^{3+i\psi}w^{3+i\psi}(u+v+w-2)^{3-i\psi}}$$
$$\times(u-1)\,[(u-6v+5)\,(u-1)^2 + (9u-2v-7)\,(v-1)^2$$
$$-(2u-v-1)\,(u+v-3w+1)\,(w-1)]\,dw\,dv\,du. \tag{D 4}$$

Appendix E

In this Appendix we determine the analytical solution of the amplitude equations at the parametric resonance stage. The oblique-mode amplitudes are then small enough so that we can neglect the self-interaction term in (5.50) and the nonlinear interaction terms in (5.51) to obtain

$$\frac{\mathrm{d}\tilde{A}}{\mathrm{d}\bar{x}} = \tfrac{4}{5}\tilde{A} + \frac{2\mathrm{i}}{5}\int_{-\infty}^{\bar{x}} (\bar{x}-x_1)^2 \tilde{A}_0(x_1)\tilde{A}^*(2x_1-\bar{x})\,\mathrm{d}x_1, \tag{E 1}$$

$$\frac{\mathrm{d}\tilde{A}_0}{\mathrm{d}\bar{x}} = (1+\mathrm{i}\tilde{\kappa}_1)\tilde{A}_0. \tag{E 2}$$

The result can also be obtained formally by setting

$$\delta = \epsilon, \tag{E 3}$$

in place of (5.9) and following the same (but, simplified) procedure as in §5.

It follows from (E 1), (E 2), and (5.57) that

$$\tilde{A}_0 = \mathrm{e}^{(1+\mathrm{i}\tilde{\kappa}_1)\bar{x}}, \tag{E 4}$$

and, therefore, that

$$10\tilde{a}' - (13-5\mathrm{i}\tilde{\kappa}_1)\tilde{a} = \frac{\mathrm{i}}{2}\mathrm{e}^{\bar{x}}\int_{-\infty}^{\bar{x}} (\bar{x}-x_1)^2 \tilde{a}^*(x_1)\,\mathrm{d}x_1, \tag{E 5}$$

where we have put

$$\tilde{a} = \mathrm{e}^{(1-\mathrm{i}\tilde{\kappa}_1)\bar{x}'^2}\tilde{A}. \tag{E 6}$$

Substituting the assumed expansion

$$\tilde{a} = \mathrm{e}^{\tau\bar{x}} \sum_{n=0}^{\infty} a_n \exp\{[n-(-1)^n \tfrac{1}{2}\mathrm{i}\tilde{\kappa}_1]\bar{x}\} \tag{E 7}$$

into this result and reordering the indices of summation shows that

$$\sum_{n=1}^{\infty} [a_n\{10(\tau+n)-13+[1-(-1)^n]\,5\mathrm{i}\tilde{\kappa}_1\} - \tfrac{1}{2}\mathrm{i}C_{n-1}a_{n-1}^*]\exp\{[n-(-1)^n\tfrac{1}{2}\mathrm{i}\tilde{\kappa}_1]\bar{x}\} = 0, \tag{E 8}$$

provided we take

$$\tau = \tfrac{13}{10}, \tag{E 9}$$

where

$$C_n \equiv \int_{-\infty}^{0} \eta^2 \exp\{[\tau+n+(-1)^n\tfrac{1}{2}\mathrm{i}\tilde{\kappa}_1]\eta\}\,\mathrm{d}\eta = \frac{2}{[\tau+n+(-1)^n\tfrac{1}{2}\mathrm{i}\tilde{\kappa}_1]^3} \quad \text{for} \quad n = 0, 1, 2, \ldots. \tag{E 10}$$

It follows that (E 7) will satisfy (E 5) for arbitrary a_0 if a_n satisfies the recurrence relation

$$a_n = \frac{\mathrm{i}C_{n-1}}{2[10n+\{1-(-1)^n\}5\mathrm{i}\tilde{\kappa}_1]}a_{n-1}^* \quad \text{for} \quad n = 1, 2, 3, \ldots, \tag{E 11}$$

and (E 6) and (E 7) satisfy the upstream boundary condition (5.56) when we take

$$a_0 = a^{(0)}. \tag{E 12}$$

For simplicity we restrict our attention to the perfectly tuned case where $\tilde{\kappa}_1 = 0$. Then the recurrence solution (E 11) is easily summed to obtain

$$a_n = \frac{1}{20^n n!}\mathrm{e}^{\mathrm{i}\epsilon_n\phi}(C_0 C_1 C_2 \ldots C_{n-1})a^{(0)}, \tag{E 13}$$

where
$$\epsilon_n = \begin{cases} 1, & n = 1,3,5,\ldots, \\ 0, & n = 2,4,6,\ldots, \end{cases} \tag{E 14}$$

and we have put
$$\phi = \arg[\mathrm{i}a^{(0)*}/a^{(0)}]. \tag{E 15}$$

It follows that
$$\tilde{a} = [\tfrac{1}{2}(a_+ + a_-) + \tfrac{1}{2}\mathrm{e}^{\mathrm{i}\phi}(a_+ - a_-)]\,a^{(0)} \tag{E 16}$$

where
$$a_\pm \equiv \mathrm{e}^{\tau\bar{x}}\left[\sum_{n=1}^{\infty}\left(\frac{\pm\mathrm{e}^{\bar{x}}}{20}\right)^n \frac{(C_0 C_1 \ldots C_{n-1})}{n!} + 1\right]. \tag{E 17}$$

Equation (E 17) becomes
$$a_\pm = \mathrm{e}^{\tau\bar{x}} \sum_{n=0}^{\infty}\left(\frac{\pm\mathrm{e}^{\bar{x}}}{10}\right)^n \frac{1}{n![(\tau)_n]^3}, \tag{E 18}$$

where $(\tau)_n \equiv \Gamma(\tau+n)/\Gamma(\tau)$ denotes the generalized factorial function, and $\Gamma(\tau)$ denotes the gamma function. It is also of interest to determine the asymptotic behaviour of (E 16) as $\bar{x} \to \infty$. Now it is shown in Dingle (1973, p. 86) that

$$\cos(\pi Z)\frac{1}{\Gamma^2(Z)} = -\frac{1}{2\pi\mathrm{i}}\int_\infty^{(0+)} \frac{J_0(-2U)}{(-U)^{2Z}}\,U\,\mathrm{d}U, \tag{E 19}$$

where J_0 denotes the zeroth-order Bessel function in the usual notation and $\int_\infty^{(0+)}$ denotes the integration over the contour starting from a point at ∞ on the positive real axis, encircling the origin once counterclockwise and returning to the starting position. Then since the Bessel function $J_{\tau-1}(Z)$ has the representation

$$J_{\tau-1}(Z) = \mathrm{i}^{1-\tau}\sum_{n=0}^{\infty}\frac{(\frac{1}{2}\mathrm{i}Z)^{2n+\tau-1}}{n!\,\Gamma(\tau+n)}, \tag{E 20}$$

it follows from (E 18) that the $a_\pm$ have the integral representations

$$a_\pm \sim \frac{\mathrm{e}^{\tau\bar{x}}}{2\pi\mathrm{i}}\Gamma^3(\tau)\int_\infty^{(0+)}(-U(\pm\tfrac{1}{10})^{\frac{1}{2}}\mathrm{e}^{\bar{x}/2})^{1-\tau}J_{\tau-1}\left(2(\pm\tfrac{1}{10})^{\frac{1}{2}}\frac{\mathrm{e}^{\bar{x}/2}}{U}\right)J_0(-2U)\frac{1}{U}\mathrm{d}U, \tag{E 21}$$

or upon introducing the new variable

$$s = U/(\pm\tfrac{1}{10}\mathrm{e}^{\bar{x}})^{\frac{1}{4}}, \tag{E 22}$$

$$a_\pm \sim \frac{\Gamma^3(\tau)}{2\pi}\mathrm{e}^{\tau\bar{x}}(\pm\tfrac{1}{10}\mathrm{e}^{\bar{x}})^{3(1-\tau)/4}\,\mathrm{i}^{1-2\tau}\int_\infty^{(0+)} s^{-\tau}J_{\tau-1}\left[\frac{2}{s}(\pm\tfrac{1}{10}\mathrm{e}^{\bar{x}})^{\frac{1}{4}}\right] \times J_0[-2s(\pm\tfrac{1}{10}\mathrm{e}^{\bar{x}})^{\frac{1}{4}}]\,\mathrm{d}s, \tag{E 23}$$

which for large $\bar{x}$ becomes

$$a_\pm \sim \frac{\Gamma^3(\tau)}{2\pi^2}\mathrm{e}^{\tau\bar{x}}(-1)^{1-\tau}(\pm\tfrac{1}{10}\mathrm{e}^{\bar{x}})^{(2-3\tau)/4}\int_\infty^{(0+)} s^{-\tau}\cos\left[\frac{2}{s}(\pm\tfrac{1}{10}\mathrm{e}^{\bar{x}})^{\frac{1}{4}} - \tfrac{1}{2}\tau\pi + \tfrac{1}{4}\pi\right] \times \cos[-2s(\pm\tfrac{1}{10}\mathrm{e}^{\bar{x}})^{\frac{1}{4}} - \tfrac{1}{4}\pi]\,\mathrm{d}s. \tag{E 24}$$

This integral has saddle points at

$$s = \pm 1, \pm\mathrm{i} \tag{E 25}$$

and it follows that

$$a_\pm \sim \frac{\Gamma^3(\tau)}{2(2\pi)^{\frac{3}{2}}}\mathrm{e}^{\mathrm{i}\pi/4}(\pm\tfrac{1}{10}\mathrm{e}^{\bar{x}})^{3(1-2\tau)/8}\mathrm{e}^{\tau\bar{x}}\exp[4(\pm\tfrac{1}{10}\mathrm{e}^{\bar{x}})^{\frac{1}{4}}] \quad \text{as} \quad \bar{x}\to\infty, \tag{E 26}$$

which shows that $\tilde{A}$ grows like the exponential of an exponential as $\bar{x}\to\infty$.

REFERENCES

BENNEY, D. J. & BERGERON, R. F. 1969 A new class of nonlinear waves in parallel flows. *Stud. Appl. Maths* **48**, 181–204.

CHENG, H. K. & SMITH, F. T. 1982 The influence of airfoil thickness and Reynolds number on separation. *Z. Angew. Math. Phys.* **33**, 151–180.

CRAIK, A. D. D. 1971 Non-linear resonant instability in boundary layers. *J. Fluid Mech.* **50**, 393–413.

DINGLE, R. B. 1973 *Asymptotic Expansions: Their Derivation and Interpretation.* Academic.

GAJJAR, J. & SMITH, F. T. 1985 On the global instability of free disturbances with a time-dependent nonlinear viscous critical layer. *J. Fluid Mech.* **157**, 53–77.

GEAR, C. W. 1971 *Numerical Initial Value Problems in Ordinary Differential Equations.* Prentice-Hall.

GOLDSTEIN, M. E. & CHOI, S. W. 1989 Nonlinear evolution of interacting oblique waves on two-dimensional shear layers. *J. Fluid Mech.* **207**, 97–120. Also Corrigendum, *J. Fluid Mech.* **216**, 659–663.

GOLDSTEIN, M. E., DURBIN, P. A. & LEIB, S. J. 1987 Roll-Up of vorticity in adverse-pressure-gradient boundary layers. *J. Fluid Mech.* **183**, 325–342.

GOLDSTEIN, M. E. & HULTGREN, L. S. 1988 Nonlinear spatial evolution of an externally excited instability wave in a free shear layer. *J. Fluid Mech.* **197**, 295–330.

GOLDSTEIN, M. E. & LEIB, S. J. 1989 Nonlinear evolution of oblique waves on compressible shear layers. *J. Fluid Mech.* **207**, 73–96.

GRAEBEL, W. P. 1966 On determination of the characteristic equations for the stability of parallel flows. *J. Fluid Mech.* **24**, 497–508.

HICKERNELL, F. J. 1984 Time-dependent critical layers in shear flows on the beta-plane. *J. Fluid Mech.* **142**, 431–449.

KACHANOV, YU. S. & LEVCHENKO, V. YA. 1984 The resonant interaction of disturbances at laminar–turbulent transition in a boundary layer. *J. Fluid Mech.* **138**, 209–247.

KLEBANOFF, P. S., TIDSTROM, K. D. & SARGENT, L. M. 1962 The three-dimensional nature of boundary-layer instability. *J. Fluid Mech.* **12**, 1–34.

KOPAL, Z. 1961 *Numerical Analysis*, 2nd edn. Chapman & Hall.

LANDAU, L. D. & LIFSHITZ, E. M. 1987 *Fluid Mechanics*, 2nd edn. Pergamon.

LEIB, S. J. 1991 Nonlinear evolution of subsonic and supersonic disturbances on a compressible free shear layer. *J. Fluid Mech.* **224**, 551–578.

LIN C. C. 1955 *The Theory of Hydrodynamic Stability.* Cambridge University Press.

MILES, J. W. 1962 A note on the inviscid Orr–Sommerfeld equation. *J. Fluid Mech.* **13**, 427–432.

NIELD, D. A. 1972 On the inviscid solutions of the Orr–Sommerfeld equation. *Math. Chronicle* **2**, 43–52.

RAETZ, G. S. 1959 A new theory of the cause of transition in fluid flows. Northrop Corp. NOR-59-383 BLC-121.

REID, W. H. 1965 The stability of parallel flows. In *Basic Developments in Fluid Dynamics* (ed. M. Holt), Vol. 1, pp. 249–307. Academic.

SCHLICHTING, H. 1979 *Boundary-Layer Theory*, 7th edn. McGraw-Hill.

SMITH, F. T. & BODONYI, R. J. 1982 Nonlinear critical layers and their development in streaming-flow stability. *J. Fluid Mech.* **118**, 165–185.

SMITH, F. T. & STEWART, P. A. 1987 The resonant-triad nonlinear interaction in boundary-layer transition. *J. Fluid Mech.* **179**, 227–252.

STEWARTSON, K., SMITH, F. T. & KAUPS, K. 1982 Marginal separation. *Stud. Appl. Maths* **67**, 45–61.

STUART, J. T. 1960 On the non-linear mechanics of wave disturbances in stable and unstable parallel flows. Part 1. The basic behaviour in plane Poiseuille flow. *J. Fluid Mech.* **9**, 353–370.

WATSON, J. 1960 On the non-linear mechanics of wave disturbances in stable and unstable parallel flows. Part 2. The development of a solution for plane Poiseuille flow and for plane Couette flow. *J. Fluid Mech.* **9**, 371–389.